π-π scattering and $\pi^+ d$ interactions at 7 GeV/c*

J. T. Carroll and J. A. J. Matthews
Stanford Linear Accelerator Center, Stanford University, Stanford, California 94305

W. D. Walker
Duke University, Durham, North Carolina 27706

M. W. Firebaugh
University of Wisconsin, Parkside, Kenosha, Wisconsin 53140

J. D. Prentice and T. S. Yoon
University of Toronto, Toronto, Ontario, Canada
(Received 27 March 1974)

Using bubble-chamber data on the reactions $\pi^+ d \to p_s p \pi^0 \pi^0$, $\pi^+ d \to p_s p \pi^+ \pi^-$, and $\pi^- p \to n \pi^+ \pi^-$ at 7 GeV/c incident π momentum, π-π phase shifts are determined for $0.6 < M(\pi\pi) < 1.5$ GeV/c^2. An $I=0$ S-wave resonance is observed in the f^0 peak region of $M(\pi\pi)$. Constructive ρ-ω interference is found in the reaction $\pi^+ n \to p \pi^+ \pi^-$ and evidence is presented for some specifically deuteron effects in the data with large spectator-proton momentum.

I. INTRODUCTION

In the last decade there has been great interest in studies of the reaction $\pi\pi \to \pi\pi$. The elastic scattering of identical spinless particles attracts inquiry in part due to its ultimate simplicity. In this paper we report on a study of both elastic and inelastic π-π scattering.

We study the reactions

$$\pi^+ d \to p_s p + \text{neutrals}, \tag{1}$$

$$\pi^+ d \to p_s p \pi^+ \pi^- \tag{2}$$

as observed in a deuterium-filled bubble chamber exposed to a 7 GeV/c π^+ beam. The feature of reaction (1) in which we are most interested is the reaction

$$\pi^+ d \to p_s p \pi^0 \pi^0 . \tag{3}$$

This reaction allows one to study the π-π system in a state restricted to even values of spin l and isotopic spin I. We are able to reconstruct reaction (3) using γ rays from the π^0 decay which were converted in two $\frac{1}{8}$-in. tantalum plates mounted at the downstream end of the chamber. The dominant feature of the missing-mass spectrum from reaction (1) is the f^0 meson. In addition to an f^0 signal, reaction (2) shows strong ρ^0 and g^0 resonance production.

Reactions (1) and (2) have previously been studied in bubble-chamber experiments with an incident π^+ beam momentum of 2.7,[1] 3.65,[2] 4.5,[3] 5.1,[4] 6.0,[5] and 9.0 GeV/c.[6] In addition there have been some $\pi^+ d$ experiments with $P_{\text{lab}} \simeq 2$ GeV/c searching for the ϵ^0 meson.[7] The charge-conjugate reaction to reaction (3),

$$\pi^- p \to n \pi^0 \pi^0 , \tag{4}$$

has been studied using spark chambers to measure the γ directions from the π^0 decay.[8]

The outline of this paper is as follows. In Sec. II we discuss our data on reactions (1) and (3). Our experimental procedure is outlined and results on the elastic charge-exchange reaction $\pi^+ n \to p \pi^0$ are presented. We discuss the missing-mass spectrum from reaction (1) and determine the cross section for $f^0 \to$ all neutrals. Our procedure for reconstructing the $2\pi^0$ system using the measured γ directions is then introduced (see also the Appendix) and the fitted $2\pi^0$ events are used to study the $M(p\pi^0)$ mass spectrum.

In Sec. III we discuss our data on reaction (2). Cross sections and resonance parameters for ρ^0, f^0, and g^0 production are obtained and compared with the data of Oh *et al.*[9] for the reaction

$$\pi^- p \to n \pi^+ \pi^- \tag{5}$$

at 7 GeV/c. In Sec. IV we determine π-π phase shift parameters for $0.6 < M(\pi\pi) < 1.5$ GeV/c^2 by fitting the $\pi^+ \pi^-$ angular distributions using an absorption-modified one-pion-exchange (AOPE) model. For this purpose we combine our data from reaction (2) with that of Oh *et al.*[9] for reaction (5). We discuss the inelasticity of the $I=0$ D wave using data on the non-2π decay modes of f^0 meson. In Sec. V we present evidence for constructive ρ-ω interference in the reaction (2) 4-prong data. The π-nucleon mass spectra in reactions (2) and (5) are examined in Sec. VI, and

some effects arising from our use of a deuteron target are discussed in Sec. VII.

II. $\pi^+ d \to p_s p$ + NEUTRALS

The 7-GeV/c $\pi^+ d$ film analyzed in this experiment was obtained in a 650 000-picture exposure of the Midwestern Universities Research Association Argonne National Laboratory 30-in. bubble chamber using the 7° separated beam from the ZGS (zero-gradient synchrotron).[10,11] Each roll of film was scanned once within a specified fiducial volume for 2-prong events for which both tracks were identifiable protons. All events were examined by an editor (an experienced scanner with special training) who checked the identification of the tracks, checked for stopping tracks, and estimated the proton ionization. The editor also checked the tantalum plates for associated $\gamma \to e^+e^-$ pairs, checked the alignment of the γ's with the vertex of the event, and estimated a lower limit on the γ energy. The editor took a 35-mm photograph of each good event, which was used to locate the γ's for measuring. The events were measured manually on film plane digitizers and all 2-prong events were processed using the DIANA[12] spatial reconstruction and kinematic fitting program. The fits were checked for consistency between the calculated and scanner-estimated ionization.

For all events with (missing mass)$^2 < 0.5$ GeV^2 we tried the 1-constraint (1C) hypothesis

$$\pi^+ d \to p_s p \pi^0 . \tag{6}$$

Figures 1(a) and 1(b) show the missing-mass and χ^2 distributions for 2-prong events accepted as fitting this reaction. Of the 250 events which fitted reaction (6), 36% had a 3-constraint fit using the measured γ directions. This implies an over-all γ-detection efficiency of 0.6 for γ's which hit the plates with enough energy ($\gtrsim 0.2$ GeV) to produce a visible shower. For these single π^0 events the average π^0 momentum is 6.8 GeV/c and the average $\gamma\gamma$ opening angle is 3.0°, so the fraction of γ's missing the plates is negligible. Figure 1(d) is a plot of $M(\gamma\gamma)$ from the 2C fit $\pi^+ d \to p_s p \gamma_1 \gamma_2$; the π^0 peak is 10 MeV wide. In Fig. 1(c) we have plotted the ratio E_{γ_1}/E_{π^0}. There is a slight deviation from the expected flat distribution.

We find the elastic charge-exchange cross section at 7 GeV/c to be 67 ± 10 μb as shown in Table I. This cross section is corrected for 1-prong events (spectator proton unseen) but no allowance has been made for our upper cutoff of 1.3 GeV/c on proton momentum [apart from Fermi motion smearing this corresponds to $t \simeq -1.25$ (GeV/c)^2]. In Fig. 2(a) we have plotted the elastic charge-exchange cross section for reaction (6) vs P_{lab}.

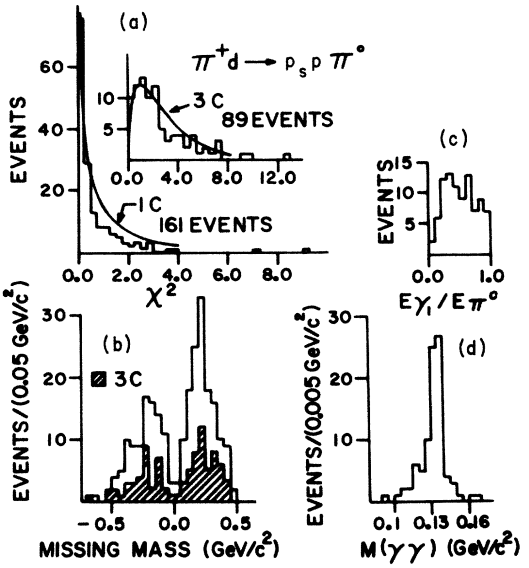

FIG. 1. Event characteristics for $\pi^+ d \to p_s p \pi^0$. (a) χ^2 distributions for 1-constraint (1C) and 3-constraint (3C) fits; (b) missing-mass distribution; (c) the ratio E_{γ_1}/E_{π^0} for 3C fits where γ_1 is the first of two measured γ's; (d) $M(\gamma\gamma)$ for 3C fits.

Our value seems to be consistent with measurements of the charge-conjugate reaction $\pi^- p \to \pi^0 n$.[13] Also shown are measurements of $\sigma(\pi^+ n \to \pi^0 p)$ at 4.5,[3] and 6 GeV/c.[5] Figure 2(b) is a plot of $d\sigma/dt$ for our elastic events. Fitting the data from 0.12 to 0.6 (GeV/c)^2, we find an exponential falloff with slope $\simeq 10$ (GeV/c)$^{-2}$ in agreement with the results of Wahlig *et al.*[14] for $\pi^- p \to \pi^0 n$ at both 6 and 10 GeV/c. The turnover in the distribution at small t is also seen in $\pi^- p \to \pi^0 n$. Also shown in Fig. 2(b) are the low-t data points corrected for Pauli exclusion assuming all spin nonflip and using the Hulthén wave function to describe the deuteron form factor.[15] The differential cross section (with no correction for Pauli exclusion) is given in Table II.

In Fig. 3 we show the missing-mass (MM) spectrum with single π^0 events excluded and with spectator momentum (a) $|\vec{p}_s| \leq 0.3$ GeV/c and (b) $|\vec{p}_s| > 0.3$ GeV/c. The latter plot shows little evidence

TABLE I. 2-prong cross sections in 6.95-GeV/c $\pi^+ d$ interactions.

Reaction	Spectator momentum (GeV/c)	σ (μb)
$\pi^+ d \to p_s p \pi^0$	$\lvert\vec{p}_s\rvert \leq 0.3$	67 ± 10
	> 0.3	12 ± 5
$\pi^+ d \to p_s p$ + MM($\geq 2m_{\pi^0}$)	$\lvert\vec{p}_s\rvert \leq 0.3$	620 ± 60
	> 0.3	60 ± 10
$\pi^+ d \to p_s p f^0$ ($f^0 \to$ all neutrals)	$\lvert\vec{p}_s\rvert \leq 0.3$	120 ± 20
$\pi^+ d \to p_s \Delta^+(1236) \pi^0$, $\Delta^+ \to p\pi^0$	$\lvert\vec{p}_s\rvert \leq 0.3$	13 ± 5

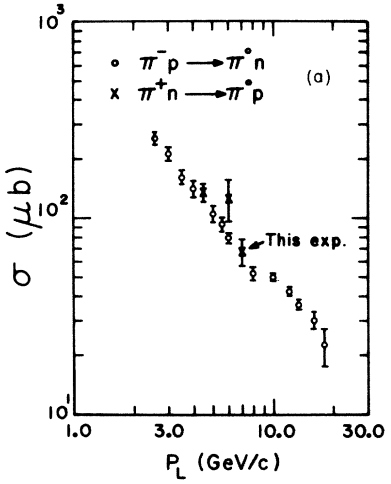

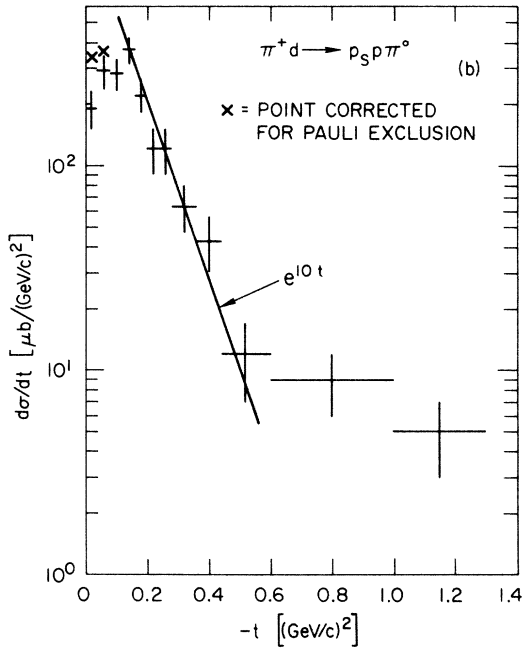

FIG. 2. (a) Elastic charge-exchange cross section vs laboratory beam momentum (P_L). The $\pi^- p$ data are from Ref. 13 and the 4.5 and 6.0 GeV/c $\pi^+ n$ cross sections are from Ref. 3 and 5. (b) Differential cross section for $\pi^+ d \rightarrow p_s p \pi^0$ with $|\vec{p}_s| < 0.3$ GeV/c. Pauli exclusion correction assuming all spin nonflip is indicated by ×.

of the resonant structure so prominent in the former distribution. (A similar effect in the $\pi^+ d \rightarrow pp\pi^+\pi^-$ data is shown in Figs. 28 and 29.) In agreement with the impulse approximation we will discard events with $|\vec{p}_s| > 0.3$ GeV/c, and this cut will always be understood unless there is an explicit statement to the contrary. The dominant feature of the missing-mass plot is the f^0 at 1.26 GeV/c^2. Below the f^0 there is an η^0 signal at 0.548 GeV/c^2 and a slight enhancement between 0.7 and 0.85 GeV/c^2 from the neutral decay of the ω^0.

TABLE II. Forward differential cross section for $\pi^+ n \rightarrow p\pi^0$ at 6.95 GeV/c.

$\lvert t \rvert$ (GeV^2)	$\frac{d\sigma}{dt}$ (μb/GeV^2)
$\lvert t_{min} \rvert - 0.04$	190 ± 40
0.04 – 0.08	290 ± 55
0.08 – 0.12	280 ± 50
0.12 – 0.16	370 ± 55
0.16 – 0.20	220 ± 40
0.20 – 0.24	120 ± 30
0.24 – 0.28	120 ± 30
0.28 – 0.36	64 ± 16
0.36 – 0.44	43 ± 13
0.44 – 0.60	12 ± 5
0.60 – 1.00	9 ± 3
1.00 – 1.30	5 ± 2

There is also some indication of structure above the f^0 at 1.65 GeV/c^2. We estimate our mass resolution near the f^0 to be 0.05 GeV/c^2.

The Chew-Low plot for these missing-mass events is shown in Fig. 4. Most of the events, especially at the f^0, are concentrated at low t (π^+ – missing mass), while the flatter t distributions in the η and ω mass regions are quite apparent. In the missing-mass distribution, Fig. 3, we observe that demanding $|t| < 0.2$ (GeV/c)^2 removes most of the η and ω peaks but leaves a

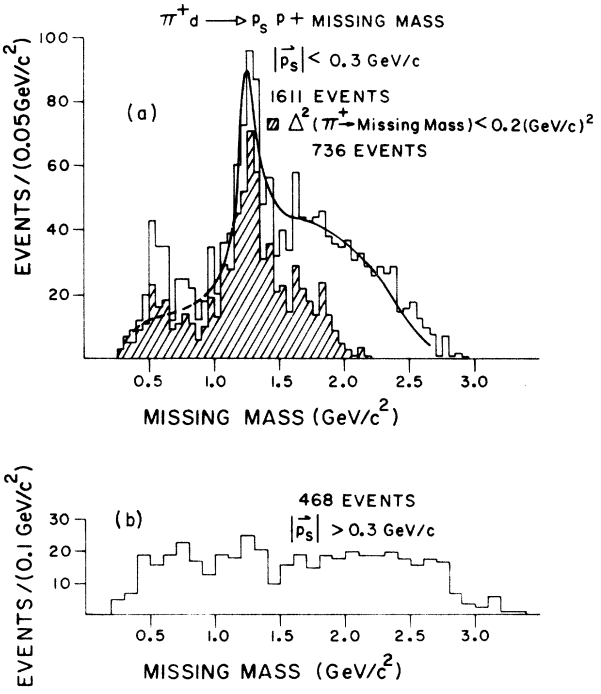

FIG. 3. Missing mass (MM) from $\pi^+ d \rightarrow p_s p$ + neutrals with single π^0 events excluded. (a) MM for $|\vec{p}_s| < 0.3$ GeV/c; (b) MM for $|\vec{p}_s| > 0.3$ GeV/c.

strong f^0 signal. In the Chew-Low plot there seems to be an excess of events at larger $|t|>0.2$ (GeV/c)^2 just above the f^0 peak, probably from $A_2^0 \to \eta^0 \pi^0$. Since we have only measured protons up to 1.3 GeV/c, there is an effective upper cutoff at $|t| \simeq 1.25$ (GeV/c)^2. Because we are working in deuterium, the Chew-Low boundary is not sharp.

The total cross section for reaction (1) with MM $\geq 2m_\pi$ is 620 ± 60 μb as shown in Table I. Comparing this result with other $\pi^+ d$ experiments,[3-5] we find the 2-prong missing-mass cross section is falling as $\sim P_{\text{lab}}^{-0.9}$ at our energy. For MM $\lesssim 1.0$ GeV/c^2 the $3\pi^0$ phase space is negligible; thus to estimate cross sections for reaction (3) we need only to correct for the neutral decay modes of the η^0 and ω^0. These corrections have been made by using known branching ratios together with our determination of η^0 and ω^0 production cross sections in the reaction

$$\pi^+ d \to p_s p \pi^+ \pi^- \pi^0. \qquad (7)$$

The dashed line below 0.9 GeV/c^2 in Fig. 3(a) shows the result of making these corrections.

We have determined the f^0 cross section by fitting the missing-mass distribution above 0.9 GeV/c^2 using a Breit-Wigner resonance form for the f^0.[16] The best fit, as shown in Fig. 3(a), used a background of roughly equal amounts of peripheral $2\pi^0$ and $3\pi^0$ phase space. We also made a subtraction for $A_2 \to \eta^0 \pi^0$ based on data from reaction (7).[17,18] The most obvious failure of the fit is the inability to fit the high side of the f^0. We find

$$M(f^0) = 1.26 \pm 0.01 \text{ GeV}/c^2,$$

$$\Gamma(f^0) = 0.18 \pm 0.03 \text{ GeV}/c^2,$$

$$\sigma(f^0) = 120 \pm 20 \ \mu\text{b}.$$

In missing-mass data at 5.1 GeV/c Armenise *et al.*[4] found $M(f^0) = 1.27$ and $\Gamma(f^0) = 0.188$ GeV/c^2.[19] Our cross section of 120 μb for $\pi^+ n \to p f^0$ is for $f^0 \to$ all neutrals. The cross section for $\pi^+ n \to p f^0$ with $f^0 \to \pi^0 \pi^0$ is somewhat smaller since the f^0 has other all neutral decay modes (see Sec. IV).

Figure 5 shows momentum transfer ($-t$) distributions for mass intervals below, at, and above the f^0. We have fitted the events in the f^0 region to an exponential distribution of the form $e^{\beta t}$. Fit-

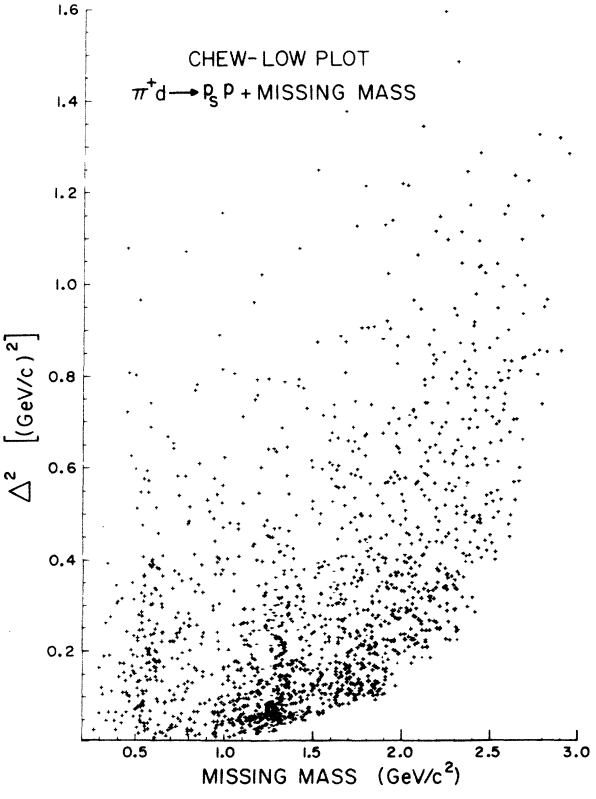

FIG. 4. Chew-Low plot of Δ^2 ($\pi^+ \to$ missing mass) vs missing mass for 2-prong events with $|\vec{p}_s| < 0.3$ GeV/c.

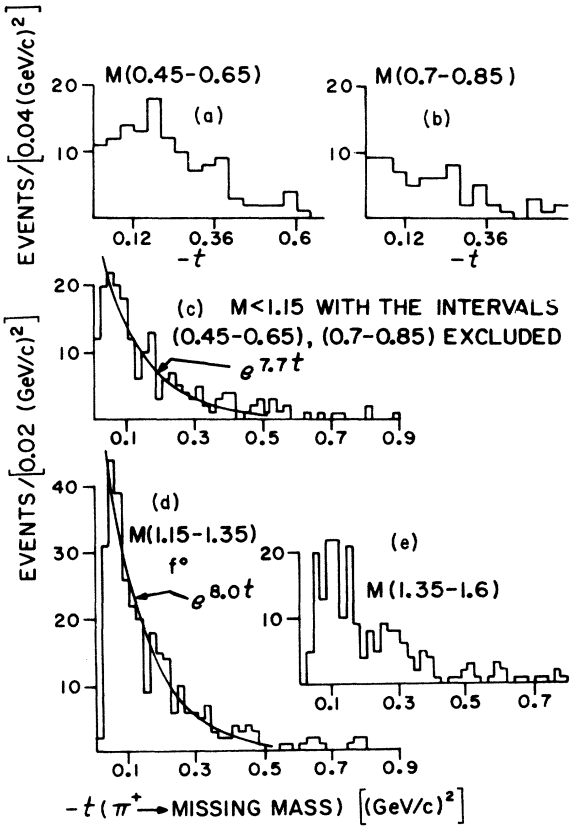

FIG. 5. Momentum transfer (t) distributions for $\pi^+ d \to p_s p$ + missing mass. (a) $0.45 <$ MM < 0.65 GeV/c^2; (b) $0.7 <$ MM < 0.85 GeV/c^2; (c) MM < 1.15 GeV/c^2 with η^0 and ω^0 regions excluded; (d) $1.15 <$ MM < 1.35 GeV/c^2; (e) $1.35 <$ MM < 1.6 GeV/c^2.

ting the data with $0.04<|t|<0.5$ $(\mathrm{GeV}/c)^2$ we find a slope $\beta=8.0\pm1.3$ $(\mathrm{GeV}/c)^{-2}$ as shown in Fig. 5(d). The CERN experiment at 5.1 GeV/c [4] found a corresponding slope of $\beta=8.8\pm1.7$ $(\mathrm{GeV}/c)^{-2}$ (they fit the t interval 0.04–0.28). For the f^0 in reaction (2) we find an exponential slope of 10.0 ± 1.0 $(\mathrm{GeV}/c)^{-2}$ for the t distribution in the mass interval $1.18<M(\pi^+\pi^-)<1.34$ GeV/c^2. The lower value of the slope in the missing-mass data can come from non-$2\pi^0$ events, for example: $A_2^0\to\eta^0\pi^0$ or $3\pi^0$.

If we observe all four γ's from the $2\pi^0$ decay in reaction (3), we have an ordinary 2C fit. Because of our limited γ detection efficiency (see the Appendix) most $2\pi^0$ events do not yield four observed γ's. In Fig. 6 the missing mass is plotted according to the number of γ's measured. An upper limit of 6 was imposed on the number of measured γ's per event (≈0.003 of the events had more than 6 associated γ's). Only 10% of the events have no observed γ's while 32% have two γ's. The f^0 is quite apparent in all five categories of γ's measured in Fig. 6.

In order to fit the events with less than 4 γ's we must make some approximations, since ordinarily these events would be underconstrained. The opening angle for the decay of a particle of mass μ and momentum p_π into two γ's satisfies the inequality $\tan\frac{1}{2}\theta\geq\mu/p_\pi$. As p_π increases $\theta_{\min}$ decreases and the opening angle distribution becomes sharply peaked near $\theta_{\min}$. Our procedure has been to construct artificial π^0 tracks constrained to lie on cones of half-angle $\approx1.25\theta_{\min}/2$ about the measured γ direction. For the 2γ and 3γ events the fitting was done using these artificial π^0 tracks. For 1γ events we simply point π_1^0 in the γ direction and calculate the direction of π_2^0. This fitting procedure and our γ detection efficiency are discussed in the Appendix.

Figure 7(b) shows the fitted $M(\pi^0\pi^0)$ for events with 1, 2, 3, and 4 γ's. Except for a more rapid falloff at large $M(\pi\pi)$ the structure of the spectrum is basically the same as the missing-mass plot. The fitting procedure with less than 4 γ's does not improve the mass resolution. Peaks at the η^0 and ω^0 are apparent. Most of the η^0 events come from $\eta^0\to3\pi^0$, since we have extracted the 2γ fits. The fitting procedure yields no discrimination against $3\pi^0$ events for $M(3\pi^0)\lesssim1.0$ GeV/c^2. In order to achieve such discrimination the individual π^0's must have sufficient transverse momentum to be well separated in the Ta plates. Our method offers no hope of distinguishing between $\pi^0\gamma$ and $2\pi^0$ unless we see all 3γ's from the $\pi^0\gamma$ decay. Consequently, the structure from 0.7 to 0.85 GeV/c^2 is consistent with $\omega^0\to\pi^0\gamma$.

We have chosen to include the 1γ fits even though these events provide no discrimination against $3\pi^0$ and have an angular resolution slightly worse

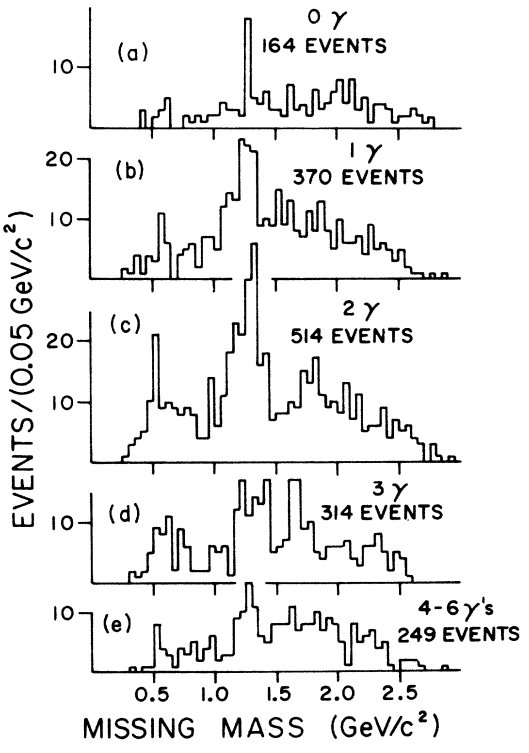

FIG. 6. Missing mass from $\pi^+d\to p_sp$ +neutrals for different γ topologies (No. of associated γ's observed in the tantalum plates). (a) 0 γ; (b) 1 γ; (c) 2 γ's; (d) 3 γ's; (e) 4 or more γ's.

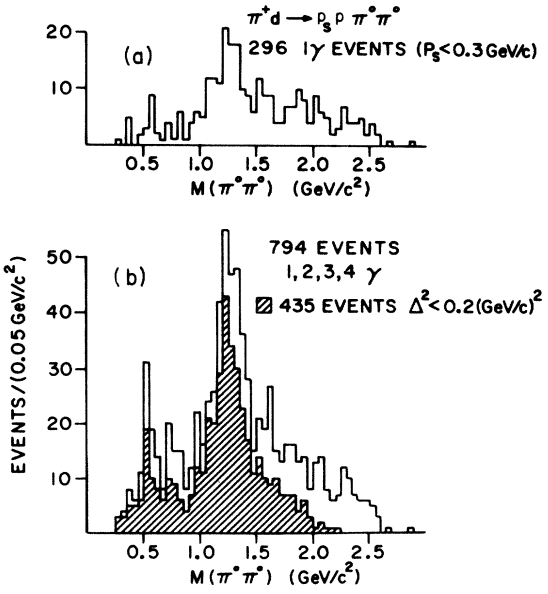

FIG. 7. $M(\pi^0\pi^0)$ from $\pi^+d\to p_sp\pi^0\pi^0$ fitted events. (a) 1γ events (0C fit); (b) 1–4 γ events.

than the 2γ, 3γ, and 4γ events. There are two factors motivating this decision. First, the details of the fitted 1γ mass and angular distributions are nearly the same as for the 2γ, 3γ, and 4γ fits. Although the 1γ mass plot, Fig. 7(a), has more events above $M(\pi\pi) = 1.5$ GeV/c^2, this is not a serious drawback since we are mostly interested in the region at and below the f^0. Second, by using the 1γ fits we avoid having to correct the fitted distributions for the absence of these events. We can also ignore, to a first approximation, any biases introduced by the fitting program efficiency—a genuine $2\pi^0$-2γ event which failed to fit would probably fit with only 1γ.

Using our fitted $2\pi^0$ events we examine the $M(p\pi^0)$ mass spectrum. $M(p\pi_1^0)$ and $M(p\pi_2^0)$ defined such that $|t(\pi^+ \to \pi_2^0)| < |t(\pi^+ \to \pi_1^0)|$ are shown in Figs. 8(a) and 8(b). In $M(p\pi_1^0)$ we see what appears to be the $\Delta^+(1236)$, particularly in the plot with $|t(\pi^+ \to \pi_2^0)| < 0.2$ GeV/c^2 (see for comparison Figs. 23 and 24). While the peak position is slightly high, a Monte Carlo study of our fitting procedure showed no systematic shift in $M(p\pi^0)$. In the insert, Fig. 8(c), we plot $M(\pi^0\pi^0)$ for events in the

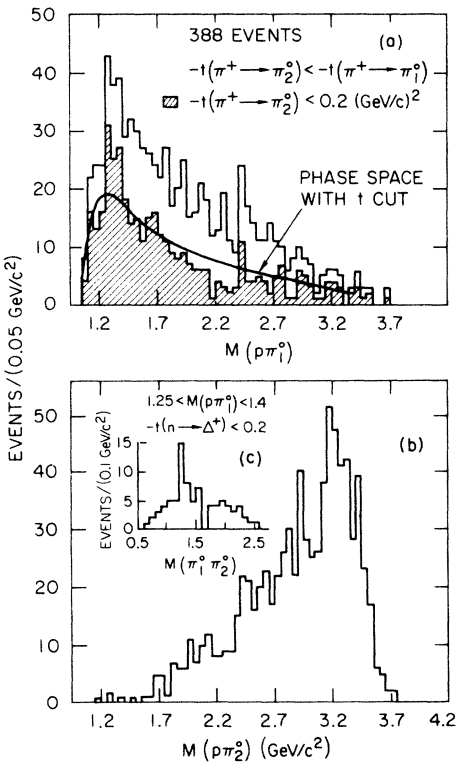

FIG. 8. (a) $M(p\pi_1^0)$ for $\pi^+ d \to p_s p\pi_1^0\pi_2^0$ with π_1^0 defined by a momentum transfer cut; (b) $M(p\pi_2^0)$; (c) $M(\pi_1^0\pi_2^0)$ for events with $M(p\pi_1^0)$ near the $\Delta^+(1236)$ and $|t(\pi^+ \to \pi_2^0)| < 0.2$ (GeV/c)^2.

Δ^+ band. There is a peak at 1.3 GeV/c^2 from the overlap of the f^0 and Δ^+, otherwise the structure is quite smooth. Correcting for the fitting program efficiency (see the Appendix), we estimate a cross section of 13 ± 5 μb for Δ^+ production in reaction (3). This compares favorably with a predicted cross section for $\pi^+ n \to \Delta^+\pi^0$ in reaction (3) of 20 ± 10 μb from data on $\pi^- p \to p\pi^-\pi^0$ at 7 GeV/c.[9]

III. $\pi^+ d \to p_s p\pi^+\pi^-$

The film was scanned for all three-prong events with one proton and four-prong events with one or two protons identifiable by ionization ($|\vec{p}| \lesssim 1.5$ GeV/c). This scanning selection implies that the four-prong events are essentially unbiased as regards target proton momentum, whereas the three-prong events have an upper cutoff on target proton momentum at $|\vec{p}| \simeq 1.5$ GeV/c. For the 4-prongs 1.6% of the events have a proton with momentum larger than 1.5 GeV/c. The three- and four-prong events were processed with the BRAVE-TVGP-SQUAW-ARROW system of programs. For the three-prong events we used the standard constraint on the unseen spectator proton as provided by SQUAW. The optical data, beam constraint, etc. were the same as used for the two-prong events. For most of these events the best fit was selected on the basis of highest constraint class and lowest χ^2. For the three-prongs we also demanded that the fitted spectator momentum projected onto the x-y plane (z is along the optic axis) be less than 0.1 GeV/c. A detailed discussion of the experimental procedure can be found in Refs. 10 and 11.

We find a total cross section of 0.95 ± 0.07 mb for reaction (2) with $|\vec{p}_s| < 0.3$ GeV/c (see Table III). This cross section agrees well with what one would predict from lower-energy $\pi^+ d$ experiments.[3-5] However, our result is 30% smaller than the cross section found for the charge-conjugate reaction (5) and the difference is too large to be accounted for simply by Glauber screening; a correction of 3% is used for screening. In fact, our analysis suggests that a substantial part of this discrepancy may be attributed to three sources. First, the Pauli exclusion principle at small momentum transfers suppresses the $\pi^+ n$ cross section by $\gtrsim 6\%$ (a lower bound obtained by as-

TABLE III. $\sigma(\pi^+ d \to p_s p\pi^+\pi^-)$ at 6.95 GeV/c.

Topology	Events	σ (μb)
3-prong	4122	589
4-prong ($\|\vec{p}_s\| < 0.3$ GeV/c)	2532	361
4-prong ($\|\vec{p}_s\| > 0.3$ GeV/c)	477	68 ± 6
Total ($\|\vec{p}_s\| < 0.3$ GeV/c)	6654	950 ± 70

suming pure spin flip at the nucleon vertex). Second, the $\pi^+ d$ scanning criteria cause the high-momentum-transfer events to be lost. A direct comparison of $\pi^+ n$ and $\pi^- p$ data indicates that the $\pi^+ n$ cross section should be scaled up by the factor 1.06 ± 0.02. Finally, a correction factor of 1.07 ± 0.01 is required to account for the abnormally large number of deuterium events with spectator momenta ≥ 0.3 GeV/c (see Table III), possibly a result of secondary interactions with the spectator nucleon.

As shown in Fig. 9 the $\pi^+\pi^-$ mass spectrum is dominated by ρ^0, f^0, and g^0 production. For the 4-prong events we have demanded $|\vec{p}_s| < 0.3$ GeV/c. The relative heights of the ρ^0 and f^0 peaks are the same for the 3- and 4-prong sets of data. Our mass resolution is 10 MeV near the f^0 peak. We have fitted the combined 3- and 4-prong data with $M(\pi^+\pi^-) < 2.1$ GeV/c^2 to 2π phase space and Breit-Wigner resonance forms for the ρ, f, and g (see Ref. 18 for a description of the fit procedure). The resulting fit is shown in Fig. 9 with $M(\pi^+\pi^-)$ in 20-MeV bins. The high-mass sides of the ρ and f are not fitted very well. The mass plot shows what appear to be shoulderlike structures on the high side of these peaks. The fit to the g^0 is poor, mostly because the mass and width of the g are not well determined by the data.

Resonance parameters and cross sections as determined by this fit are given in Table IV. Also shown in Table IV are the corresponding parameters for the 7-GeV/c $\pi^- p$ data using the same fitting procedure. Our ρ^0 cross section is consistent with what one would predict from lower-energy $\pi^+ d$ experiments assuming a P_{lab}^{-2} energy dependence. We find the ratio

$$\frac{\sigma(f^0 \to \text{all neutrals})}{\sigma(f^0 \to \pi^+\pi^-)} = 0.47 \pm 0.09$$

in good agreement with lower-energy $\pi^+ d$ experiments at 3.65 [2] and 5.1 GeV/c.[4]

In Fig. 10 we plot the momentum transfer, t, from the beam to the $\pi^+\pi^-$ system for various π-π mass intervals in the $\pi^+ d$ data. The forward differential cross sections for ρ^0 and f^0 production in the combined $\pi^- p$ and $\pi^+ d$ data are given in Table V. Both the $\pi^- p$ and $\pi^+ d$ data show a break in the t distribution at $|t| \simeq 0.25$ (GeV/c)^2. Fitting the $\pi^+ d$ distributions for $|t| < 0.24$ (GeV/c)^2 to an exponential of the form $e^{\beta t}$ we find a slope β in the range 11–14 (GeV/c)$^{-2}$ for all mass intervals shown in Fig. 10. The corresponding exponential slopes from the 7 GeV/c $\pi^- p$ data are with one exception within errors of the $\pi^+ d$ values. The exception is for $1.34 < M(\pi\pi) < 1.42$ GeV/c^2 where the $\pi^- p$ data give $\beta = 7.4 \pm 2.9$. From comparison with

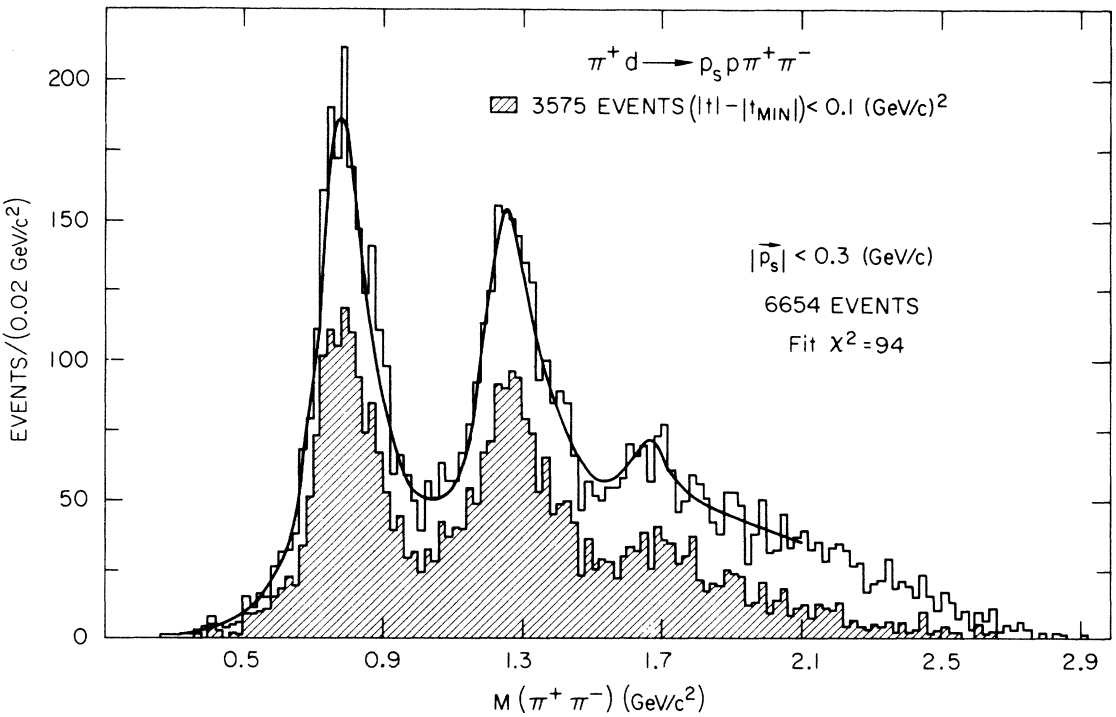

FIG. 9. $M(\pi^+\pi^-)$ from $\pi^+ d \to p_s p \pi^+ \pi^-$ with $|\vec{p}_s| < 0.3$ GeV/c. The curve results from a fit using Breit-Wigner resonance forms for the ρ^0, f^0, and g^0.

TABLE IV. Resonance parameters and production cross sections in $\pi N \to N\pi^+\pi^-$.

Expt.	Resonance	Mass (GeV/c^2)	Γ (GeV/c^2)	σ (μb)
$\pi^+ d$	ρ^0	0.780±0.003	0.165±0.010	352±70
$\pi^+ d$	f^0	1.264±0.004	0.194±0.015	258±25
$\pi^+ d$	g^0	1.68±0.01	0.16±0.04	50±20
$\pi^- p$	ρ^0	0.783±0.003	0.145±0.010	387±40
$\pi^- p$	f^0	1.274±0.005	0.170±0.020	231±30
$\pi^- p$	g^0	1.65±0.02	0.07±0.02	28±10

the $\pi^- p$ data we can make a rough estimate of the number of small-t events missing in the $\pi^+ d$ data because of Pauli exclusion. It appears that for $M(\pi^+\pi^-) \lesssim 0.9$ GeV/c^2 we lose from 30 to 45% of the events with $|t| < 0.02$ (GeV/c)^2 while the loss at larger t is negligible. This loss is consistent with Pauli exclusion assuming approximately half spin-flip and half spin-nonflip. In the f^0 region the loss of events with $|t| < 0.02$ (GeV/c)^2 is 5–10% ($|t_{\min}| \simeq 0.014$ at the f^0).

IV. π-π SCATTERING IN $\pi N \to N\pi\pi$

A. Procedure

The π-π scattering is usually parameterized in terms of phase shifts δ_l^I and inelasticities η_l^I (l = angular momentum and I = isotopic spin of the π-π system). For $M(\pi\pi) \lesssim 1.0$ GeV/c^2 the π-π phase shifts have been studied by many authors.[20-22] Recent experiments have clarified the behavior of the phase shifts in the ρ^0 mass region and provided data in and above the f^0 mass region.[23-27]

Since the reaction $\pi\pi \to \pi\pi$ cannot be studied directly, one is always dependent on a model to extract π-π scattering data from some other reaction. With the OPE model as first developed by Goebel[28] and by Chew and Low[29] the idea was to extract π-π phase shifts from the reaction $\pi N \to N\pi\pi$ by extrapolating in the variable t from the physical (off mass shell) to the unphysical (on mass shell) point at $t = m_\pi^2$. Other than direct extrapolation procedures the methods for using the OPE model to study π-π scattering fall into two general categories. The first approach, as used by Ferrari and Selleri,[30] attempts to allow for off mass shell effects by introducing form factor functions of t at the upper and lower vertices of the OPE diagram. Dürr and Pilkuhn modified this procedure by adding angular momentum barrier penetration factors to the vertex function, and Benecke and Dürr did a relativistic Dürr-Pilkuhn treatment.[31]

The second method of modifying the simple OPE model is to adjust the formalism so as to take into account the strong absorption of the low partial waves in the entrance and exit channels of the reaction. In the absorption-modified one-pion-exchange model (AOPE) as originally developed by Gottfried and Jackson[32] the absorption in the initial and final states is approximated as being similar to elastic π-nucleon scattering. In our analysis

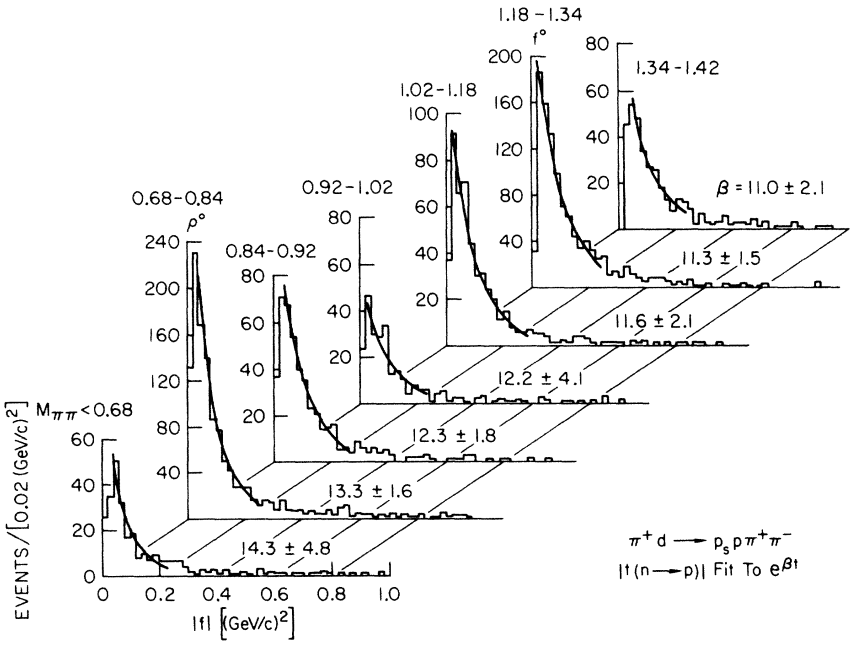

FIG. 10. Momentum transfer (t) distributions in $\pi^+ d \to p_s p \pi^+ \pi^-$ for various $M(\pi^+\pi^-)$ intervals. The curves result from fits to the data with $0.04 < |t| < 0.24$ (GeV/c)^2 yielding exponential slopes, β, as shown.

TABLE V. Forward differential cross sections for $\pi N \to \rho^0 N'$ and $\pi N \to f^0 N'$ at 6.95 GeV/c.[a]

$\pi N \to \rho^0 N'$[b]		$\pi N \to f^0 N'$[c]	
$\lvert t\rvert$ (GeV^2)	$\frac{d\sigma}{dt}$ (mb/GeV^2)	$\lvert t\rvert$ (GeV^2)	$\frac{d\sigma}{dt}$ (mb/GeV^2)
$\lvert t_{min}\rvert - 0.02$	2.78 ± 0.19	$\lvert t_{min}\rvert - 0.02$	2.05 ± 0.27
0.02 – 0.04	3.56 ± 0.21	0.02 – 0.04	2.45 ± 0.15
0.04 – 0.06	2.36 ± 0.14	0.04 – 0.06	1.94 ± 0.11
0.06 – 0.08	1.90 ± 0.12	0.06 – 0.08	1.43 ± 0.09
0.08 – 0.10	1.44 ± 0.11	0.08 – 0.10	1.09 ± 0.08
0.10 – 0.15	0.90 ± 0.05	0.10 – 0.12	0.82 ± 0.07
0.15 – 0.20	0.49 ± 0.05	0.12 – 0.14	0.75 ± 0.07
0.20 – 0.25	0.31 ± 0.03	0.14 – 0.16	0.58 ± 0.06
0.25 – 0.30	0.22 ± 0.03	0.16 – 0.18	0.44 ± 0.05
0.30 – 0.35	0.15 ± 0.02	0.18 – 0.20	0.40 ± 0.05
0.35 – 0.40	0.11 ± 0.02	0.20 – 0.22	0.33 ± 0.04
0.40 – 0.50	0.078 ± 0.011	0.22 – 0.26	0.26 ± 0.03
0.50 – 0.60	0.080 ± 0.011	0.26 – 0.30	0.14 ± 0.02
0.60 – 0.80	0.047 ± 0.006	0.30 – 0.34	0.13 ± 0.02
0.80 – 1.00	0.024 ± 0.004	0.34 – 0.40	0.107 ± 0.014
		0.40 – 0.50	0.068 ± 0.009
		0.50 – 0.60	0.044 ± 0.007
		0.60 – 0.80	0.020 ± 0.003
		0.80 – 1.00	0.014 ± 0.003

[a]The $\pi^+ n$ data have been corrected for Pauli exclusion effects assuming pure spin flip at the nucleon vertex.
[b]The ρ^0 differential cross section is normalized to an integrated cross section of 360 μb for $\lvert t\rvert \leq 1.0$ GeV^2.
[c]The f^0 differential cross section is normalized to an integrated cross section of 250 μb for $\lvert t\rvert \leq 1.0$ GeV^2.

we have used the AOPE formalism of Durand and Chiu.[33] For a detailed discussion of our analysis see Refs. 9 and 10.

For the purpose of making a phase-shift analysis of the $\pi^+\pi^-$ system we have combined the $\pi^+ d$ data of this experiment with the 6.93-GeV/c $\pi^- p$ data[9] to obtain a total sample of 10 845 $\pi^+\pi^-$ events. For this study we use only the data with a momentum transfer $\lvert t\rvert < 0.3$ (GeV/c)^2. In Fig. 11 we plot $M(\pi^+\pi^-)$ for the 8039 events which survive this t cut. We confine our study to the mass range $0.58 < M(\pi\pi) < 1.5$ GeV/c^2. In Figs. 12 and 13 we plot

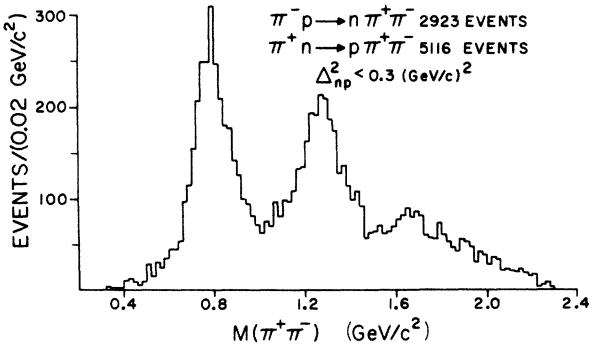

FIG. 11. $M(\pi^+\pi^-)$ for compilation of $\pi^- p$ and $\pi^+ d$ data with $\lvert t_{np}\rvert < 0.3$ (GeV/c)^2.

the π-π scattering angles, $\cos\theta_{\pi\pi}$ and the azimuthal angle φ, in the Jackson frame. We use 40-MeV bins except for the mass range $1.22 < M(\pi^+\pi^-) < 1.34$ GeV/c^2 where we use 20-MeV bins. The angular distributions plotted separately for the $\pi^- p$ and $\pi^+ d$ data (not shown) are in good agreement. In the ρ^0 region of Fig. 12 we see the forward peaking in $\cos\theta$ resulting from the S-P wave interference. Around 1.0 GeV/c^2 there is peaking in the backward direction and above 1.14 GeV/c^2 there is a strong D-wave signal characteristic of the f^0. Near the ρ^0 the azimuthal distributions (Fig. 13) tend to peak near $\varphi = 0°$. This peaking is well described by the absorption model. Above 1.0 GeV/c^2 the data are consistent with isotropic distributions in φ. The curves in Figs. 12 and 13 are the result of fitting these angular distributions to determine π-π phase shifts.

The differential cross section for $\pi N \to N\pi\pi$ can be written in the form[9]

$$\frac{\partial^4\sigma}{\partial m_{\pi\pi}\,\partial t\,\partial\cos\theta\,\partial\varphi} = C\frac{k}{P_{lab}^2}\frac{1}{2}\sum_{\mu\lambda'\lambda}\lvert\langle\mu\lambda'\rvert T\rvert\lambda\rangle\rvert^2, \tag{8}$$

C = normalization constant,

P_{lab} = incident laboratory beam momentum,

k = momentum of outgoing π in $\pi\pi$ c.m. system,

μ = helicity of the dipion system,

λ', λ = helicity of the outgoing and incoming nucleons.

The amplitudes $\langle\mu\lambda'\rvert T\rvert\lambda\rangle$ can be expanded in terms of spherical harmonics and the π-π phase shifts. Appendix B of Ref. 9 gives explicit forms of these amplitudes with the absorption modifications as used in this analysis.[34] The only free parameters in (8) are the $\pi\pi$ phase shifts, inelasticities, and normalization constant, C.

For each π-π mass interval in Fig. 12 we made a least-squares fit to the $\cos\theta$ and φ distributions simultaneously with the phase shifts and inelasticities as the only free parameters. Normally we used bins of 0.1 in $\cos\theta$ and 18° in φ, i.e., a 20 × 10 matrix. For a given trial set of phase-shift parameters we performed a numerical integration of Eq. (8) over the t interval $\lvert t\rvert_{min} < \lvert t\rvert < 0.3$ (GeV/c)^2 for each point of the 20 × 10 matrix in $\cos\theta$ and φ (the integration was carried out in terms of $\cos\theta_{c.m.}$). A fit with 27 degrees of freedom typically yielded a χ^2 of 29 to 35.

The over-all normalization in Eq. (8) was fixed so as to maximize the agreement between the fit values for δ_D^0 and the predictions of a Breit-Wigner resonance form for the f^0 in the mass range $1.25 < M(\pi^+\pi^-) < 1.32$ GeV/c^2. Good agreement can only

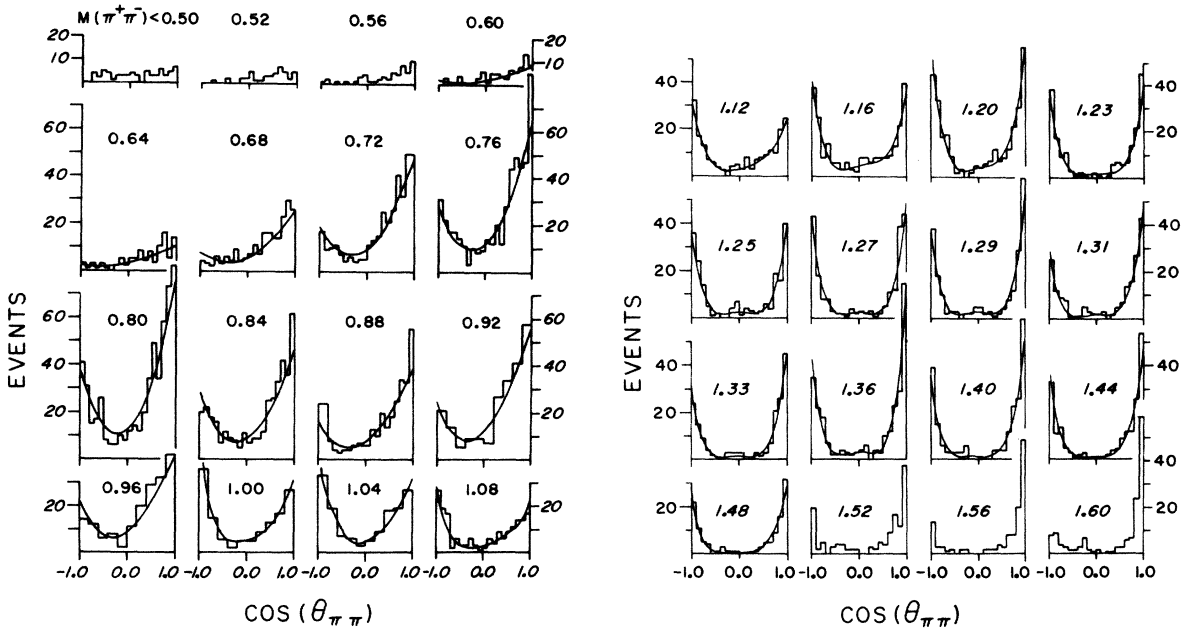

FIG. 12. $\cos\theta_{\pi\pi}$ (Jackson angle) distributions for combined $\pi^+ n$ and $\pi^- p$ data with $|t|<0.3$ (GeV/c)^2. Central values are shown for the 40 MeV/c^2 bins in $M(\pi^+\pi^-)$. The bin size is 0.1 in $\cos\theta$ except for $0.90<M(\pi^+\pi^-)<1.06$ GeV/c^2 where the bin size is 0.2. The solid curves show the AOPE model fit results.

be obtained on the low-mass side since we find the $I=0$ D wave to be significantly inelastic at and above the f^0 peak. We estimate that this procedure allows the normalization to be determined to $\approx 10\%$. In order to obtain values of δ_P^1 at the ρ^0 peak in good agreement with a Breit-Wigner resonance form we had to use a normalization 13% larger than that found at the f^0 peak. For $M(\pi^+\pi^-)<0.98$ GeV/c^2 we have used the larger normalization found at the ρ^0 peak. Occasionally we have constrained a particular parameter so as to maintain reasonable continuity from one mass bin to the next; usually this was not necessary and the solutions were unique.

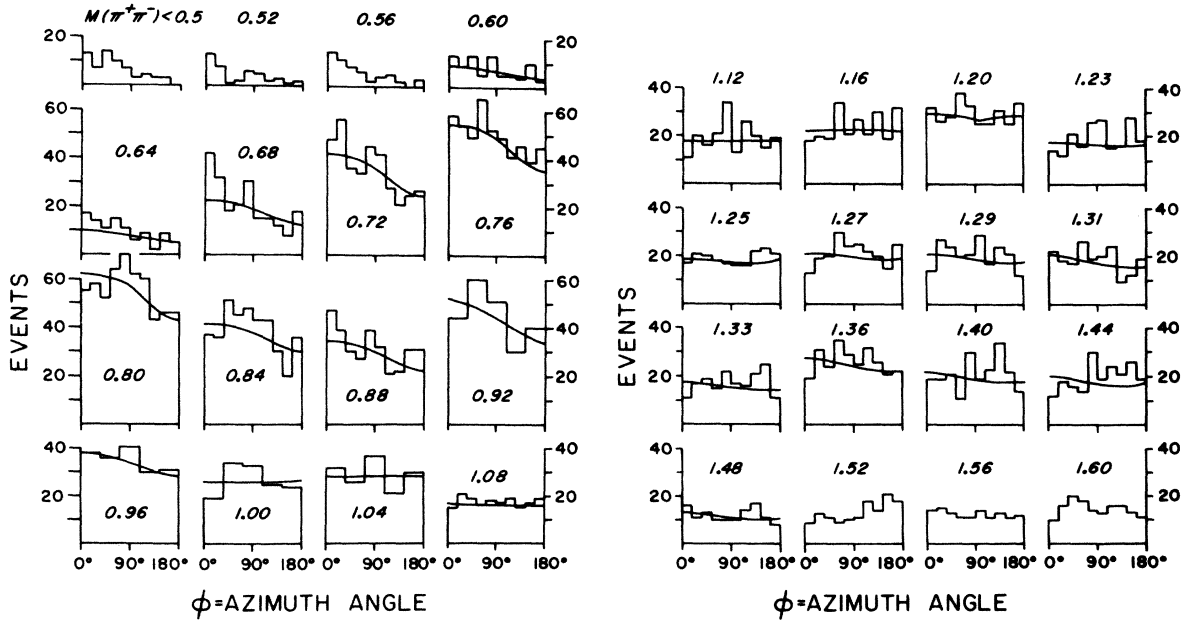

FIG. 13. Azimuth (Treiman-Yang) angle for 40 MeV/c^2 bins in $M(\pi^+\pi^-)$. The bin size is 18° in φ except for $0.90<M(\pi^+\pi^-)<1.06$ GeV/c^2 where the bin size is 36°. The solid curves show the AOPE model fit results.

B. $I = 2$ phase shifts

The $\pi^+\pi^-$ data are rather insensitive to the $I=2$ phase shifts and inelasticities: η_S^2, δ_S^2, η_D^2, and δ_D^2. To fit the $\pi^+\pi^-$ angular distributions we have fixed the $I=2$ parameters at values determined from the reaction

$$\pi^- p \to p\pi^-\pi^0 . \tag{9}$$

For $M(\pi^+\pi^-) < 1.2$ GeV/c^2 we used the $I=2$ phase shifts of Baton *et al.*[22] as shown in Fig. 14. Our $\pi^+\pi^-$ data in this mass region support these results. Studies of the reaction[35]

$$\pi^- d \to pp\pi^-\pi^-$$

also support the general features of the $I=2$ analysis of Baton *et al.* In Fig. 15 we plot π-π angular distributions for reaction (9) from the data of Oh *et al.*[9] with $P_{\text{lab}} = 6.93$ GeV/c. Fitting these data in 80 MeV bins for $0.98 < M(\pi^-\pi^0) < 1.22$ GeV/c^2, we find that the resulting δ_S^2 and δ_D^2 also agree with the phase shifts determined by Baton *et al.*

To determine the $I=2$ parameters above 1.2 GeV/c^2 we have fitted the $\pi^-\pi^0$ angular distributions from the 6.93 GeV/c data as shown in Fig. 15. The over-all normalization has been adjusted so as to maximize the agreement between our fit results and those of Baton *et al.* in the mass range $0.98 - 1.22$ GeV/c^2. The P-wave parameters were fixed so as to agree with the $\pi^+\pi^-$ fit results. The resulting fits to the $\pi^-\pi^0$ angular distributions are shown in Fig. 15, and the fit parameters η_S^2, δ_S^2, and δ_D^2 are plotted with error bars in Fig. 14. Although the data are consistent with $\eta_D^2 = 1.0$ for

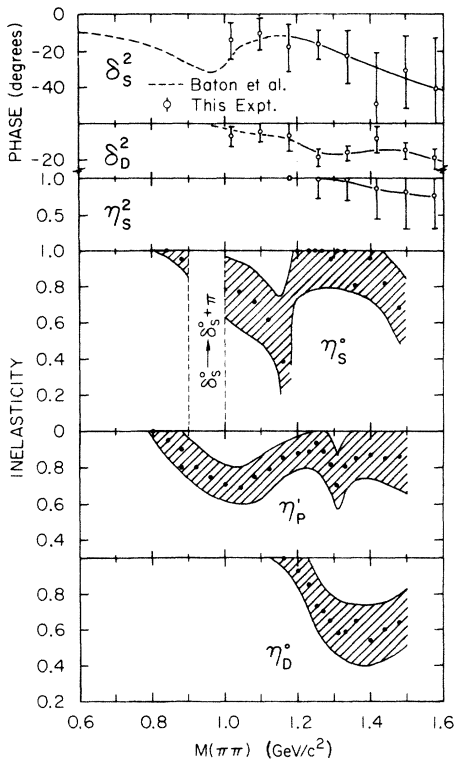

FIG. 14. π-π phase shifts and inelasticities δ_S^2, δ_D^2, η_S^2, η_S^0, η_P^1, and η_D^0 from the AOPE model fits to the $\pi^+\pi^-$ and $\pi^-\pi^0$ angular distributions. The data of Baton *et al.* are from Ref. 22. The shaded bands indicate roughly the area between the upper and lower limits. The break in η_S^0 for $0.9 < M(\pi\pi) < 1.0$ GeV/c^2 indicates the region where δ_S^0 has been shown to rise rapidly through 90° (see Ref. 24).

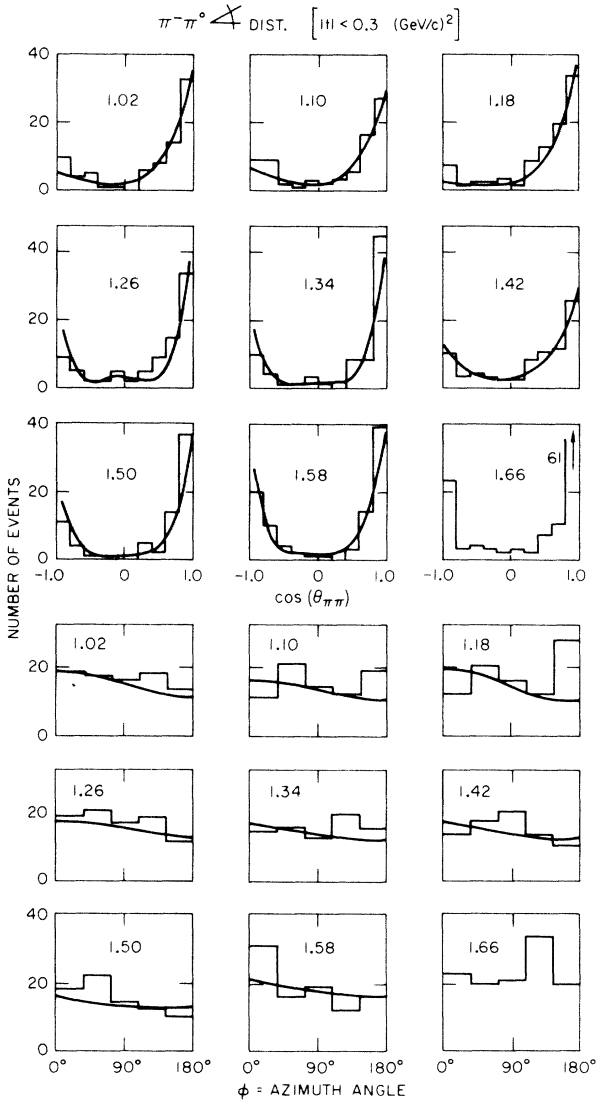

FIG. 15. π-π angular distributions for $\pi^- p \to p\pi^-\pi^0$ with $|t| < 0.3$ (GeV/c)^2. Central values are shown for the 80 MeV/c^2 bins in $M(\pi^-\pi^0)$ and the curves show the results of the AOPE model fits.

$M(\pi\pi) < 1.58$ GeV/c^2, we cannot rule out the possibility that η_D^2 is somewhat smaller than 1.0 above 1.46 GeV/c^2. Above 1.2 GeV/c^2 we find δ_S^2 is falling steadily and gradually becoming inelastic. The errors are large since in addition to limited statistics we must contend with a low S-wave unitarity bound. The D wave, δ_D^2, is relatively constant near $-16°$ for $1.25 < M(\pi\pi) < 1.55$ GeV/c^2. For the purpose of fitting the $\pi^+\pi^-$ data we have used the smooth curves drawn through the fitted results above 1.2 GeV/c^2 in Fig. 14.

C. The ρ^0 region: $M(\pi^+\pi^-) < 1.0$ GeV/c^2

For the purpose of discussing the $\pi^+\pi^-$ fit results we consider the data above and below 1.0 GeV/c^2 separately. This division is prompted by the dominance of the resonant parameters δ_P^1 and δ_D^0 for $M(\pi^+\pi^-)$ below and above 1.0 GeV/c^2. With the $I=2$ phase shifts fixed as discussed above we fit the $\pi^+\pi^-$ angular distributions in the ρ^0 mass region with the $I=0$, 1 phase shifts and inelasticities as the only free parameters. The resulting best-fit parameters are shown in Figs. 14 and 16.

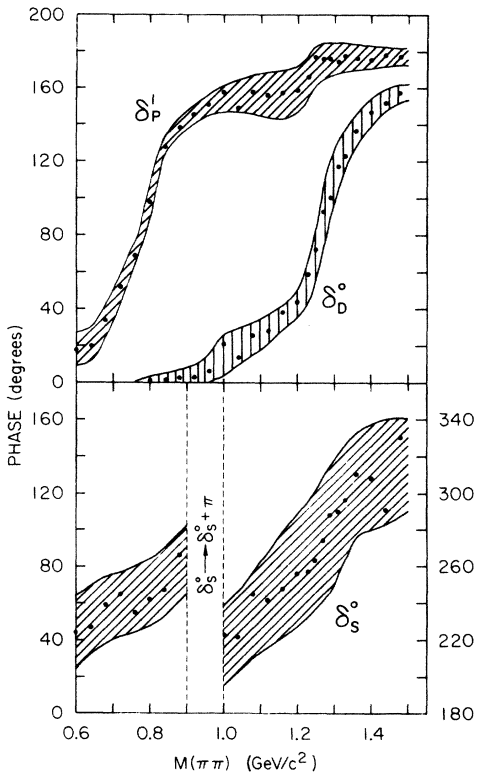

FIG. 16. π-π phase shifts δ_S^0, δ_P^1, and δ_D^0 from the AOPE model fits to the $\pi^+\pi^-$ angular distributions. The shaded bands indicate roughly the area between the upper and lower limits. The break in δ_S^0 for $0.9 < M(\pi\pi) < 1.0$ GeV/c^2 indicates the region in which δ_S^0 rises rapidly through 90° (see Ref. 24).

The AOPE model fits well the general deviation from isotropy in the azimuthal angle distributions. Some details of the $\cos\theta$ distributions such as the sharp forward peaking near $\cos\theta_{\pi\pi} = 1.0$ are poorly fit. A previous analysis which included nucleon-pole terms in the production amplitude was also unable to fit this forward peaking.[9]

The fit $I=0$, 1 phase-shift parameters are tabulated in Table VI. The quoted errors for δ_l^I are usually taken from the least-squares fit. Occasionally the fitting program has trouble determining the error for a particular fit parameter, e.g., δ_D^0 near 0° in the 0.8–1.0 GeV/c^2 region. In such cases the errors have been estimated from fits with the particular parameter in question fixed at various trial values. The error estimates for η_D^0 have usually been found in the same manner, i.e., by trial and error. Because η_l^I and δ_l^I are usually highly correlated the fitting program has difficulty determining reasonable errors for these two parameters simultaneously. The quoted errors do not include the $\approx 10\%$ uncertainty in the over-all normalization; however, we note that a change in the normalization of $\approx 12\%$ at the f^0 peak moves δ_S^0 and δ_D^0 by 5–6°.

The various families of $I=0$ S-wave phase shifts in the ρ^0 mass region have been the subject of considerable controversy in the literature. The up-up set of phase shifts as shown in Fig. 17(a) was originally proposed by Hagopian and Selove.[36] This solution received support in the work of Malamud and Schlein,[37] and Gutay *et al.*[38] The now accepted up-down family was first proposed by Walker *et al.*[39] Several experiments on the $2\pi^0$ system including this one now clearly indicate that the up-down solution is correct in the ρ^0 region (e.g., Bensinger *et al.*[7]). The Berkeley experiment of Protopopescu *et al.*[24] which showed a sudden jump in δ_S^0 in the 900–950 MeV mass range, finished any controversy regarding the S wave in the ρ^0 region. In Figs. 14 and 16 we have indicated that δ_S^0 rises rapidly through 90° by the break in the data for $0.9 < M(\pi\pi) < 1.0$ GeV/c^2, although our $\pi^+\pi^-$ data cannot resolve this behavior.

Our $2\pi^0$ data from reaction (3) also favor the down solution for δ_S^0 above the ρ^0 peak. In Fig. 17(b) we plot $d\sigma/dm_{\pi\pi}$, corrected for η^0 and ω^0 contamination, along with the prediction of Malamud and Schlein[37] for "down-up," "up-down," and "up-up" solutions for δ_S^0. For the cross-section curves of Fig. 17(b) we have used the $I=2$ S-wave phase shifts of Baton *et al.*[22] The Malamud and Schlein predictions give absolute cross sections and are not renormalized for our data. For $M(\pi^0\pi^0) \leq 0.5$ GeV/c^2, our $2\pi^0$ cross section is systematically larger than the Malamud and Schlein predictions and is inconclusive with re-

TABLE VI. π-π phase shifts and inelasticities (δ in degrees).

$M(\pi^+\pi^-)$ (GeV/c^2)	δ_S^0	η_S^0	δ_P^1	η_P^1	δ_D^0	η_D^0	δ_F^1
0.60	44±20		18±9				
0.64	47±25		20±9				
0.68	59±25		34±9				
0.72	65±20		52±7				
0.76	55±15		69±6		0		
0.80	62±15		98±10	1.0±0.05	1±3		
0.84	67±15	1.0±0.05	128±5	0.95±0.1	2±5		
0.88	86±20	0.95±0.05	138±5	0.90±0.1	3±7		
0.92			145±5	0.80±0.1	3±5		
0.96			151±5	0.75±0.1	6±4		
1.00			158±10	0.70±0.1	21±10		
1.04	222±20	0.77±0.2	149±10	0.68±0.1	14±11		
1.08	245±18	0.71±0.2	158±11	0.75±0.1	25±9		
1.12	242±25	0.62±0.15	156±12	0.79±0.1	28±10		
1.16	248±30	0.38±0.35	157±12	0.85±0.1	38±9	1.0±0.05	
1.20	256±20	1.0±0.2	159±10	0.88±0.1	44±6	0.93±0.1	
1.23	257±40	1.0±0.2	166±20	0.89±0.1	59±15	0.85±0.15	
1.25	263±30	1.0±0.2	177±7	0.94±0.15	72±10	0.73±0.15	
1.27	274±35	1.0±0.2	176±10	0.89±0.15	93±10	0.70±0.15	
1.29	288±35	.95±0.2	176±10	0.82±0.15	100±15	0.65±0.15	
1.31	290±35	1.0±0.2	174±8	0.70±0.15	117±12	0.58±0.15	
1.33	296±40	1.0±0.2	178±9	0.81±0.15	123±14	0.59±0.15	
1.36	310±17	0.80±0.2	176±5	0.85±0.15	136±7	0.65±0.2	
1.40	308±34	0.96±0.2	175±6	0.87±0.15	147±10	0.54±0.2	0±5
1.44	291±30	0.82±0.2	178±12	0.85±0.15	152±8	0.60±0.15	1.2±5
1.48	330±10	0.68±0.2	177±4	0.86±0.15	158±4	0.64±0.15	2.4±5

gard to the various solutions for δ_S^0. In the mass region from 0.7 to 0.9 GeV/c^2 our data definitely favor the "down" branch of the "up-down" or "down-down" solutions. In the interval 0.6–0.9 GeV/c^2 the "down-up," "up-down," and "up-up" solutions have a χ^2 of 12.3, 0.1, and 10.1, respectively (3 degrees of freedom). The upward curving branches of the "up-down" and "down-up" solutions above 0.9 GeV/c^2 in Fig. 17(b) show the effect of including a D wave as found in our $\pi^+\pi^-$ analysis. Below 0.9 GeV/c^2 the D-wave correction is negligible. Apparently the D wave below 1.0 GeV/c^2 is not enough to account for the failure of the "up" branch for δ_S^0.

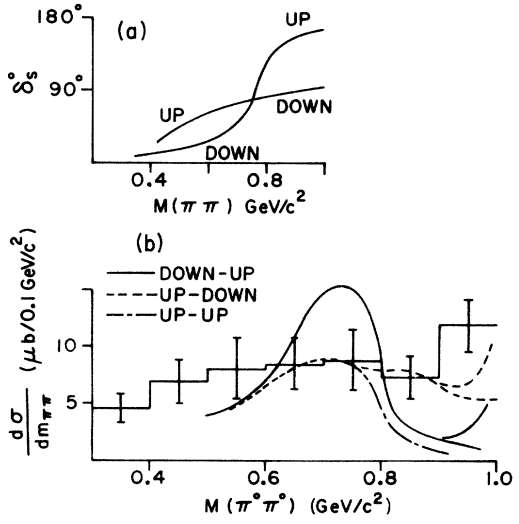

FIG. 17. (a) Diagram of four possible solutions for δ_S^0 in the ρ^0 mass region. (b) $M(\pi^0\pi^0)$ with curves showing the predictions of Malamud and Schlein (see Ref. 37). The alternate upward curving branches near 1.0 GeV/c^2 show the effect of including a small D-wave contribution.

As an additional check on the consistency of the $\pi^0\pi^0$ and $\pi^+\pi^-$ data we compare $\sigma(\pi^0\pi^0)$ with $\sigma(\pi^+\pi^-)$ in the ρ^0 peak region. Using the data for $0.7 < M(\pi\pi) < 0.8$ GeV/c^2 we find

$$\frac{\sigma(\pi^+ n \to p\pi^+\pi^-)}{\sigma(\pi^+ n \to p\pi^0\pi^0)} = 13.1 \pm 4.1 .$$

The large error results from the low statistics of the $2\pi^0$ data. Nevertheless this ratio is consistent with that expected for P wave to S wave at the unitarity limit

$$\frac{\sigma_{+-}}{\sigma_{00}} = \frac{(12 + \frac{16}{9})\pi\lambda^2}{\frac{8}{9}\pi\lambda^2} = 15.5 .$$

The $2\pi^0$ angular distributions are plotted in Fig. 18 for events which fit reaction (3) using the measured γ directions. The data shown have $|t| < 0.3$ (GeV/c)^2. We have fitted these angular distributions with δ_S^0 and δ_D^0 as free parameters and the over-all normalization adjusted so as to maximize

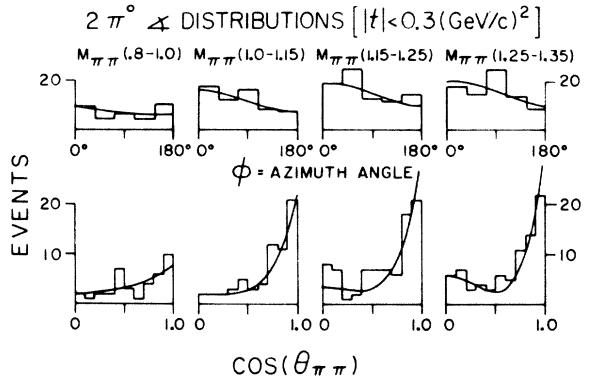

FIG. 18. $\cos\theta_{\pi\pi}$ and azimuthal angle distributions for $\pi^+ n \to p\pi^0\pi^0$. The curves show the AOPE model fit results with δ_S^0 and δ_D^0 as given in Table VII.

the agreement with δ_D^0 as determined from our $\pi^+\pi^-$ data in the f^0 peak region (i.e., at the f^0 peak only δ_S^0 is being determined by the fit). Low statistics demanded the use of large mass bins and consequently the fit is often averaging over an interval where one of the parameters is known to vary rapidly. The AOPE model fit results for δ_S^0 and δ_D^0 are given in Table VII and the curves in Fig. 18 show the resulting fits to the $2\pi^0$ angular distributions. For $0.8 < M(\pi\pi) < 1.0$ GeV/c^2 we find δ_D^0 larger than our $\pi^+\pi^-$ results (see Table VI). However, in this mass interval δ_S^0 agrees with the data of Protopopescu *et al.*[24]

D. The f^0 region

With the $I=2$ phase shifts fixed, there are six free parameters to be determined: η_S^0, δ_S^0, η_P^1, δ_P^1, η_D^0, and δ_D^0. Of these the $I=0$ S-wave parameters are most difficult to fit because of the low S-wave unitarity bound. We find that the $l=3$ partial wave, δ_F^1, becomes important only for $M(\pi\pi) > 1.4$ GeV/c^2. As shown in Fig. 16 the $I=0$ D wave, δ_D^0, rises steadily from 10° to 45° from 1.0–1.2 GeV/c^2 while δ_P^1 holds in the interval 150° to 160°. In the mass range 0.98–1.14 GeV/c^2 the $\cos\theta$ distributions of Fig. 12 become sharply peaked near $\cos\theta = -1$. This results in the negative Y_3^0 moment of the π-π angular distribution in this mass interval between the ρ^0 and f^0 peak regions.[40] In a plot of $M(\pi^+\pi^-)$ for $\cos\theta < -0.8$ we see no statistically significant structure. This backward peaking in $\cos\theta$ must be produced by the interference of two or more states of opposite parity, e.g., S-P, P-D, or S-P-D interference. Our results would favor P-D interference, i.e., a fairly constant P wave interfering with a rising D wave (Oh *et al.*[9] arrived at this same conclusion).

For $0.9 < M(\pi^+\pi^-) < 1.2$ GeV/c^2 both the S and P wave have inelasticity $\eta < 1.0$. Above 1.2 GeV/c^2 η_P^1 stays mostly in the interval 0.8–0.9 (see Fig. 14), while the S-wave inelasticity reaches a minimum near 1.16 GeV/c^2 (somewhat above $K\bar{K}$ threshold) and is consistent with $\eta_S^0 = 1.0$ near the f^0 peak. Near 1.1 GeV/c^2 the inelastic S wave is associated with the $S^*(1060)$ resonance decaying into $K\bar{K}$. From data on

$$\pi^- p \to n K^0 \bar{K}^0 \tag{10}$$

at 4 and 6.2 GeV/c, Beusch *et al.*[41] estimated $0 < \eta_S^0 \lesssim 0.6$ and δ_S^0 near 90° or 180° at the S^* peak. From a compilation of data on reactions (10) and

$$\pi^+ d \to p_s p K^+ K^-, \tag{11}$$

Diamond *et al.*[42] found that the $K\bar{K}$ system is dominated by the $I=0$ S wave in the 1.0–1.3 GeV/c^2 mass range. As shown in Fig. 14, we find $\eta_S^0 = 0.74 \pm 0.2$ for $M(\pi^+\pi^-) \simeq 1.06$ GeV/c^2.

In the lower half of the f^0 peak region, 1.14–1.28 GeV/c^2, the $\cos\theta$ distributions are nearly symmetric about $\cos\theta = 0$ and sharply peaked at $\cos\theta = \pm 1$, indicating the dominance of the Y_2^0 term. At larger $M(\pi\pi)$ there is a stronger peaking in the forward direction at $\cos\theta = \pm 1$. The azimuthal angle distributions (Fig. 13) are relatively isotropic throughout the f^0 mass region, especially in comparison to the ρ. Apparently absorptive effects are more important for the ρ than for f^0 production.[25] In the f^0 peak region we find δ_S^0 rising slowly through 270°, i.e., an S-wave resonance.[23] From a study of $\pi^+ p \to \Delta^{++}\pi^+\pi^-$ at 8 GeV/c, Beaupré *et al.*[43] found δ_S^0 near 90° at the f^0 peak, and in a π-π phase shift analysis using data on reaction (5) at 17.2 GeV/c, Estabrooks *et al.*[25] also observe a large S-wave phase at the f^0 peak. This large S-wave phase accounts for the near absence of events near $\cos\theta = 0$ at the f^0 peak.

The $2\pi^0$ data (Fig. 18) agree reasonably well with the results for δ_S^0 and δ_D^0 in the f^0 peak region. As shown in Table VII, the AOPE model fits to the $2\pi^0$ angular distributions also yield an S-wave phase shift passing through 90° near the f^0 peak. The errors given in Table VII do not include an uncertainty in the normalization of ≈25%. The

TABLE VII. $I=0$ π-π phase shifts in $\pi^+ n \to p\pi^0\pi^0$ at 6.95 GeV/c.

$M(\pi^0\pi^0)$ (GeV/c^2)	Events	δ_S^0 (degrees)	δ_D^0[a] (degrees)
0.8–1.0	38	119±38	16±10
1.0–1.15	65	256±30	20±4
1.15–1.25	84	269±26	31±9
1.25–1.35	81	319±12	104±10

[a] Partially constrained to δ_D^0 results of Table VI.

$\cos\theta$ distribution for $1.15 < M(\pi^0\pi^0) < 1.25$ GeV/c^2 has some peculiar structure and the fit δ_D^0 is $\approx 15°$ too small. Otherwise the $2\pi^0$ results for δ_D^0 agree within errors with the $\pi^+\pi^-$ data.

E. Non-2π decay modes of the f^0 and η_D^0

With regard to the inelasticity of the $I=0$ D wave, η_D^0, it is interesting to look for non-2π decay modes of the f^0. In Fig. 19(a) we plot the missing mass from reaction (1) for events with one or more γ's which failed to fit $2\pi^0$. In addition to a definite signal at the f^0 there is a broad structure around 1.7 GeV/c^2 and a general background suggestive of 3π phase space. The number of events at the f^0 is larger than expected from the fitting program inefficiency for reconstructing the $2\pi^0$ system. A Monte Carlo study of the $2\pi^0$ fitting procedure (see the Appendix) predicts ≈ 8 events above background per 50-MeV bin in the f^0 region of Fig. 19(a). From our $\pi^+\pi^-\pi^0$ data [reaction (7)] we estimate that the reaction $\pi^+ n \to p A_2^0$ with $A_2^0 \to \eta^0\pi^0$ should contribute ≈ 6 events to Fig. 19(a).[10,17] Another source of structure in Fig. 19(a) is the $K\bar{K}$ decay mode of the f^0. Diamond *et al.*[42] have estimated this branching ratio to be

$$R = \frac{\Gamma(f^0 \to K\bar{K})}{\Gamma(f^0 \to \pi^+\pi^-)} = 0.035 \pm 0.007 .$$

Events with associated V's have been excluded from the reaction (1) data. Assuming that the structure observed near 1.3 GeV/c^2 in Fig. 19(a) results from an all neutral f^0 decay mode other than $2\pi^0$, we estimate the cross section to be

$$\sigma(\pi^+ n \to p f^0, f^0 \to \text{all neutrals} \neq 2\pi^0 \text{ or } K^0\bar{K}^0) = 7.5 \pm 4\ \mu\text{b} .$$

This cross section includes the above-mentioned corrections for $A_2^0 \to \eta^0\pi^0$, $f^0 \to K^0\bar{K}^0$, and inefficiency in the $2\pi^0$ fitting.

Other possible all-neutral f^0 decay modes are $f^0 \to \eta^0\eta^0$ and $f^0 \to 4\pi^0$. Reaction (1) events with four or more measured γ's were fitted to the hypothesis

$$\pi^+ d \to p_s p \eta^0 \eta^0 , \tag{12}$$

with $\eta^0 \to \gamma\gamma$ (a two-constraint fit). In Fig. 19(b) we plot $M(\eta^0\eta^0)$ for the 15 events which fit reaction (12)—this plot includes 1-prong events. The accumulation of these events near the f^0 suggests the possibility of an $\eta^0\eta^0$ decay mode. Assuming that all of the remaining 7.5 μb in the all-neutral topology (discussed above) results from $f^0 \to \eta^0\eta^0$ yields a cross section of $\sigma(\pi^+ n \to f^0 \to \eta^0\eta^0) = 15 \pm 8$ μb. This cross section for $f^0 \to \eta^0\eta^0$ is corrected for a branching ratio of 0.711 for $\eta^0 \to$ all neutrals. However, we cannot exclued the possibility that all or part of the 7.5 μb in the all-neutral topology results from $f^0 \to 4\pi^0$.

In addition to $f^0 \to 4\pi^0$ there are two other possible 4π decay modes, $f^0 \to \pi^+\pi^+\pi^-\pi^-$ and $f^0 \to \pi^+\pi^-\pi^0\pi^0$. From a study of the reaction

$$\pi^+ d \to p_s p \pi^+\pi^+\pi^-\pi^- \tag{13}$$

at 6 GeV/c, Anderson *et al.*[44] estimated a branching ratio of $(5.5 \pm 1.0)\%$ for $f^0 \to \pi^+\pi^+\pi^-\pi^-$ (see Table VIII). In this experiment we have studied the reaction

$$\pi^+ d \to p_s p \pi^+\pi^-\pi^0\pi^0 \tag{14}$$

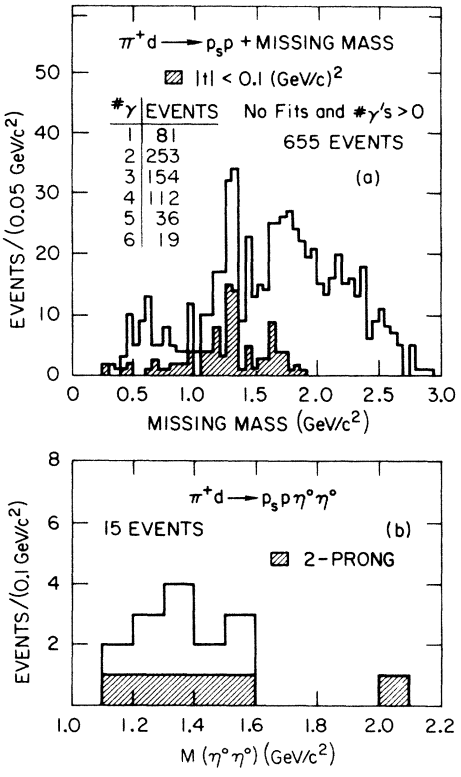

FIG. 19. (a) Missing mass for 2-prong events with one or more associated γ's which failed to fit $\pi^+ d \to p_s p \pi^0\pi^0$. (b) $M(\eta^0\eta^0)$ for 4γ events which fit $\pi^+ d \to p_s p \eta^0\eta^0$ with $\eta^0 \to \gamma\gamma$. This plot includes 1-prong events (spectator proton unseen).

TABLE VIII. Non-2π f^0 decay modes.

Decay mode (xx)	Cross section (μb)	$R = \frac{\Gamma(f^0 \to xx)}{\Gamma(f^0 \to \pi^+\pi^-)}$
$K\bar{K}$		0.035 ± 0.007[a]
$\eta^0\eta^0$	15 ± 8	0.06 ± 0.03
$\pi^+\pi^+\pi^-\pi^-$		0.055 ± 0.010[b]
$\pi^+\pi^-\pi^0\pi^0$	6 ± 3	0.02 ± 0.01

[a] Reference 42.
[b] Reference 44.

by reconstructing the $2\pi^0$ system using the measured γ directions. The $2\pi^0$ fitting procedure is basically the same as that used to study reaction (3) (see the Appendix) except that TVGP and SQUAW were used for the reconstruction and fitting. In Fig. 20 we plot $M(\pi^+\pi^-\pi^0\pi^0)$ for events with 2, 3, or 4 γ's which fit reaction (14). There appears to be some structure above background at ≈ 1.25 GeV/c^2, especially in the data with $|t_{np}| < 0.3$ (GeV/c)^2. There is also some structure in the g-meson region. In addition to $f^0 \to \pi^+\pi^-\pi^0\pi^0$ there is the possibility of $B^0(1235) \to \omega^0\pi^0$ contributing to this low-mass structure. Correcting for $B^0 \to \omega^0\pi^0$ and $A_2^0 \to \eta^0\pi^0$ we estimate[10]

$$\sigma(\pi^+ n \to p f^0, f^0 \to \pi^+\pi^-\pi^0\pi^0) = 6 \pm 3 \ \mu\text{b}.$$

This cross section must be taken as a lower limit since we have not corrected for γ conversion and $2\pi^0$ fitting program inefficiencies. However, a plot of $M(\pi^+\pi^-$ + missing mass) for events with 0 or 1 γ observed shows no evidence for structure near the f^0.

Using the estimates of non-2π f^0 decay modes summarized in Table VIII, we estimate $\eta_D^0 = 0.79 \pm 0.04$ in the f^0 peak region,[45] with $\sigma(f^0 \to \pi^+\pi^-) = 258 \pm 25$ μb and $\sigma(f^0 \to \pi^0\pi^0) = 110 \pm 20$ μb. If the f^0 peak in Fig. 19(a) is interpreted as a $4\pi^0$ decay mode instead of $f^0 \to \eta^0\eta^0$, then we obtain $\eta_D^0 = 0.82 \pm 0.03$. The error for η_D^0 is simply statistical and does not allow for any systematic error in our cross-section estimates. The π-π phase shift analysis gave a smaller value of $\eta_D^0 = 0.70 \pm 0.15$ at $M(\pi\pi) = 1.27$ GeV/c^2 (see Table VI and Fig. 14).

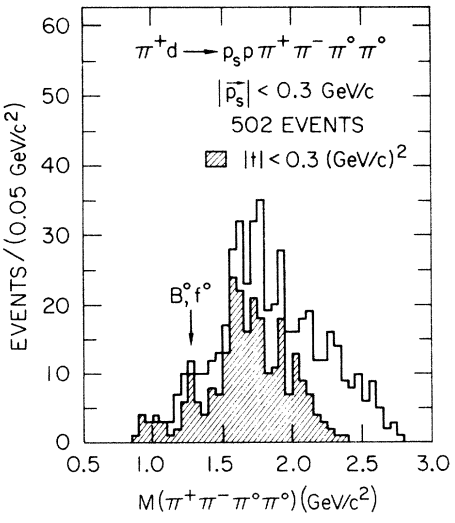

FIG. 20. $M(\pi^+\pi^-\pi^0\pi^0)$ for 4-prong events which fit $\pi^+ d \to p_s p \pi^+\pi^-\pi^0\pi^0$ with two or more measured γ's. γ's in this final state were measured and fitted for roughly $\frac{1}{2}$ of the 650000-picture exposure.

Our calculation of η_D^0 could be in error if we have neglected some non-2π decay modes of the f^0, or overestimated $\sigma(f^0 \to \pi\pi)$. It is also possible that some final states are more readily absorbed by the nucleon or deuteron than others. The above value for η_D^0 does agree within errors with the results of our π-π phase shift analysis. We conclude that the $I = 0$ D wave is significantly inelastic near the f^0 peak.

V. ρ-ω INTERFERENCE

Clear evidence for ρ-ω interference has been seen in several high-resolution, large-statistics experiments.[46] In this section we discuss the observation of ρ-ω interference in reaction (2). In Fig. 21 we plot $M(\pi^+\pi^-)$ in the ρ^0 mass region and observe a four-standard-deviation peak for $0.78 < M(\pi^+\pi^-) < 0.8$ GeV/c^2. Only 4-prong events with $|\vec{p}_s| < 0.3$ GeV/c are plotted. The 3-prong data (i.e., spectator proton unseen) show no evidence for a sharp peak near the ω mass. This difference between the 3- and 4-prong samples is compatible with the π-π mass resolution which we estimate to be 25 and 16 MeV/c^2 for the 3- and 4-prong data near the ρ^0. As shown by the shaded events in Fig. 21, most of the ω peak comes from the data with $|t| > 0.1$ (GeV/c)^2. The π-π decay angular distributions show no statistically significant differences for mass intervals below, at, and above the ω peak.

The surprising feature of Fig. 21 is the presence of a peak rather than a dip, since a Regge model based on π-B exchange degeneracy[47] predicts that we should observe destructive interference in re-

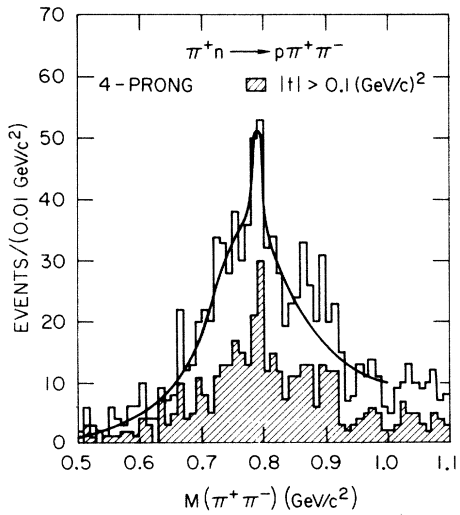

FIG. 21. $M(\pi^+\pi^-)$ for 4-prong events which fit $\pi^+ d \to p_s p \pi^+\pi^-$ with $|\vec{p}_s| < 0.3$ GeV/c. The curve shows the result of a fit with interfering Breit-Wigner amplitudes for the ρ and ω.

action (2). While our 3-prong data do not show a peak, there is no evidence for a dip in the ω region. In a 2.15 GeV/c $\pi^+ d$ experiment Bensinger and Erwin[48] also observed no indication of a dip in $M(\pi^+\pi^-)$. However, Ayres *et al.*[49] have observed destructive interference in a study of reaction (2) using the Argonne Effective Mass Spectrometer.

We have fitted the mass spectrum in Fig. 21 to a distribution similar to that used by Hagopian *et al.* and Allison *et al.*,[46] i.e., two Breit-Wigner resonance forms for the ρ and ω with a relative phase φ between them:

$$\frac{dN}{dm} = f_{ps}(m)\{A_\omega^2 |f_{BW-\omega}(m)|^2 + A_\rho^2 |f_{BW-\rho}(m)|^2 + 2\alpha A_\rho A_\omega \mathrm{Re}[e^{i\varphi} f_{BW-\omega}(m) f^*_{BW-\rho}(m)] + C\} .$$

Here $m = M(\pi^+\pi^-)$, $f_{ps}(m)$ is a phase-space factor, and the functions $f_{BW-\omega}$ and $f_{BW-\rho}$ are P-wave Breit-Wigner amplitudes for the ω and ρ, respectively.[16] A_ω and A_ρ are the (real) amplitudes for decay into $\pi^+\pi^-$, α is a coherence factor ($0 \leq \alpha \leq 1$), and C is a constant for the phase-space background.

The ρ^0 resonance parameters were fixed at $M_\rho = 0.780$ GeV/c^2 and $\Gamma_\rho = 0.18$ GeV/c^2 as found from a fit to the total $\pi^+\pi^-$ mass spectrum (including 3-prong events). For the ω we used $M_\omega = 0.790$ GeV/c^2 and $\Gamma_\omega = 0.012$ GeV/c^2. This slightly high value of M_ω improved the fit to the peak in Fig. 21; in reaction (7) we found $M_\omega = 0.784 \pm 0.014$ GeV/c^2.[50] We must also make some choice for the parameter α. Using $\alpha = 1$ corresponding to complete coherence yields a lower limit on A_ω and is the usual procedure. The phase angle φ is rather insensitive to α; changing α from 1.0 to 0.2 changed φ by only 10°. With the resonance parameters and α fixed there are four free parameters: A_ω, A_ρ, φ, and C. Performing a least-squares fit to the data from 0.5 to 1.0 GeV/c^2 we found a best fit with $\chi^2 = 58$ for 46 degrees of freedom and a phase $\varphi = -1° \pm 39°$. This result together with the ω cross section in the $\pi^+\pi^-\pi^0$ channel[50] yields a branching ratio $R(\omega \to 2\pi/\omega \to 3\pi) = (3.9 \pm 3.5)\%$. With φ fixed at 180° and all other parameters at their best-fit values we found $\chi^2 = 103$, while $A_\omega = 0$ yielded $\chi^2 = 67$. The phase does not depend critically on the ρ resonance parameters, e.g., using $M_\rho = 0.787$ GeV/c^2 gave $\varphi = +8°$, while $\Gamma_\rho = 0.17$ GeV/c^2 yielded $\varphi = -8°$. Both of these results are well within errors of the best-fit value of $\varphi = -1° \pm 39°$. With M_ω fixed at 0.784 GeV/c^2 the fit results are $\varphi = -43°$ and $R = 2.3\%$ with a fit $\chi^2 = 60$.

These results are quantitatively similar to previous observations of ρ-ω interference except that we find constructive rather than the expected destructive interference. As pointed out by Quigg[51] this anomaly could be explained by a strong natural-parity exchange contribution to ρ-ω production. The original prediction of Goldhaber *et al.*[47] of destructive interference in

$$\pi^+ p \to \Delta^{++}\pi^+\pi^- \qquad (15)$$

assumed unnatural-parity exchange. For natural-parity exchange the Regge-pole exchange-degeneracy arguments imply constructive interference for reactions (2) and (15). This would show up in the $\rho_{11} + \rho_{1-1}$ combination of the density matrix elements. While we have found a natural-parity exchange contribution to ρ^0 production with $|t| \geq 0.3$ (GeV/c)^2,[18] the ρ-ω peak in Fig. 21 comes mostly from lower t events. In Figs. 22(a) and 22(b) we plot $M(\pi^+\pi^-)$ weighted by ρ_{00} and $\rho_{11} + \rho_{1-1}$ as a function of mass. Essentially all of the ρ-ω peak structure is associated with the ρ_{00} component. It is interesting to note that Protopopescu *et al.*[24] have reported observation of constructive ρ-ω interference in reaction (15) at small momentum transfer and in the ρ_{00} state. This would be quite consistent with our results.

VI. THE π-NUCLEON SYSTEM

Although ρ and f production account for roughly $\frac{2}{3}$ of the reaction (2) events it is also interesting to consider baryon resonance production. The $M(p\pi^+)$ spectrum shows little or no evidence of any low-mass resonant structure. With the other π-nucleon combination we observe considerable structure at small $M(p\pi^-)$ in Fig. 23(a). On top of a rapidly falling OPE background there are

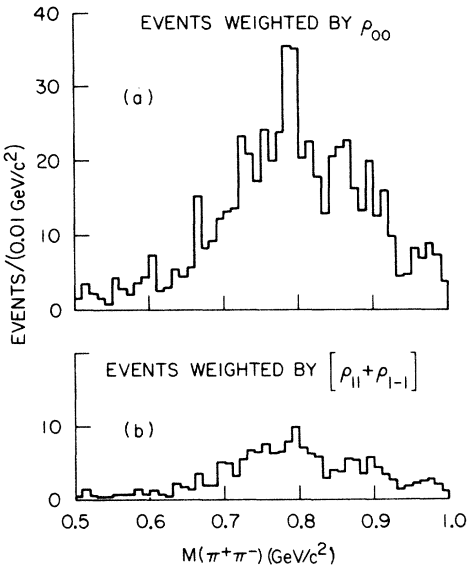

FIG. 22. $M(\pi^+\pi^-)$ for 4-prong events which fit $\pi^+ d \to p_s p\pi^+\pi^-$ with $|\vec{p}_s| < 0.3$ GeV/c. (a) $M(\pi^+\pi^-)$ weighted by ρ_{00}; (b) $M(\pi^+\pi^-)$ weighted by $\rho_{11} + \rho_{1-1}$. See Ref. 18 for density matrix elements.

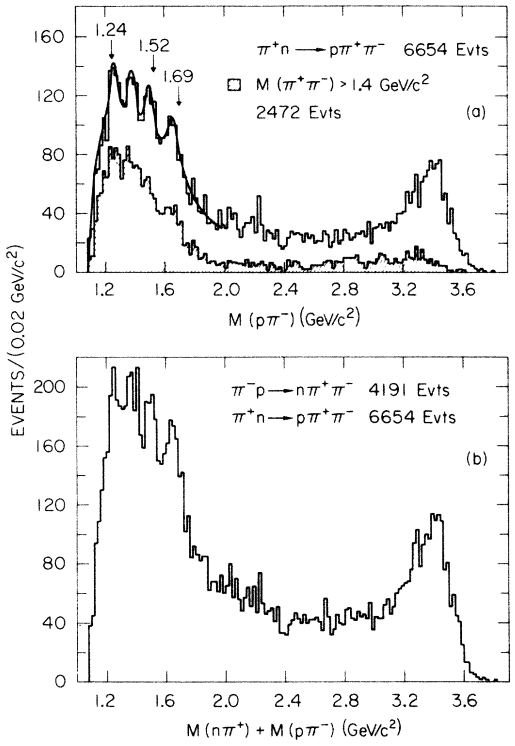

FIG. 23. $M(p\pi^-)$ for $\pi^+d \rightarrow p_s p\pi^+\pi^-$. The curve results from a fit using a handdrawn background and Breit-Wigner resonance forms for the Δ^0 and N^* peaks. (b) $M(n\pi^+)$ and $M(p\pi^-)$ for $\pi^-p \rightarrow n\pi^+\pi^-$ and $\pi^+n \rightarrow p\pi^+\pi^-$.

peaks at approximately 1.24, 1.38, 1.5, and 1.65 GeV/c^2. The location of the first peak is consistent with the $\Delta(1236)$, while the last two peaks are near the $N^*(1520)$ and $N^*(1690)$, respectively. The explanation of the peak at 1.38 GeV/c^2 is not clear since this is slightly below the usual location of the "Roper" P_{11} resonance at ≈ 1.47 GeV/c^2,[52] (this could be the result of interference).

Much of the broad structure at small $M(p\pi^-)$ is a reflection of OPE in the ρ and f regions of $M(\pi^+\pi^-)$ and perhaps the result of interference with these amplitudes. As shown in the shaded portion of Fig. 23(a), when we demand $M(\pi^+\pi^-) > 1.4$ GeV/c^2 we get a rather smoothly falling low-mass structure in $M(p\pi^-)$ with a shoulder in the 1.65-GeV/c^2 region. Momentum transfer cuts on $t_{\pi\pi}$, the four-momentum transfer from π^+_{in} to π^+_{out}, do not help to disentangle the overlap. It seems likely that some peculiar features of the π-π angular distributions (e.g., a sharp spike in the forward direction of $\cos\theta_{\pi\pi}$ near the ρ) are related to the overlap between N^* and ρ or f production.[53]

Using simple nonrelativistic Breit-Wigner resonance forms plus a hand-drawn background, we have fitted the mass distributions of Fig. 23(a) for $M(p\pi^-) < 2.0$ GeV/c^2. The resonance widths were fixed at 60–80 MeV/c^2—these rather small widths were necessary in order to reproduce the observed structure. The fitted resonance masses and cross sections are shown in Table IX (the fit $\chi^2 = 34$ for 37 degrees of freedom). The large errors reflect both the statistical uncertainty of the observed peaks and the uncertainty in the background shape. Our cross sections for $\Delta(1236)$ and $N^*(1520)$ agree with those of Anderson *et al.*,[54] who observed $\pi^-p \rightarrow \pi^-N^*$ in a missing-mass spectrum at 8 GeV/c.

In Fig. 23(b) we plot $M^* = M(n\pi^+) + M(p\pi^-)$ from the 7 GeV/c π^-p and π^+d data, respectively. The peaks at 1.24 and 1.4 GeV/c^2 are poorly defined in the $M(n\pi^+)$ distribution. The $M(p\pi^-)$ mass resolution of ≈ 8 MeV/c^2 in the low-mass region is probably somewhat better than for $M(n\pi^+)$. In Fig. 24(a) we plot M^* for $M(\pi^+\pi^-) > 1.4$ GeV/c^2 and $|t_{\pi\pi}| < 0.2$ (GeV/c)^2, and observe a broad low-mass structure suggesting a diffractive production process. For $|t_{\pi\pi}| > 0.2$ (GeV/c)^2 in Fig. 24(b) there are possible enhancements at ≈ 1.5 and 1.65 GeV/c^2. The structure from 1.6–1.7 GeV/c^2 is most definite since it persists either as a peak or a shoulder for most of the cuts that we have tried. This probably indicates that we are observing more than one resonance in this mass region. The $t_{\pi\pi}$ distributions in both experiments are well fitted by exponentials of the form $e^{\alpha t}$ where α depends on M^*, the π-nucleon mass. In Fig. 25(a) we plot α vs $M(p\pi^-)$ and find a variation of α with mass in good agreement with the $M(n\pi^+)$ data (see Ref. 9). The slope is roughly a factor of 2 smaller in the 1.5–1.7 GeV/c^2 region as compared with the 1.2–1.4 GeV/c^2 region, in agreement with the data of Anderson *et al.*[54] In Fig. 25(b) we plot α for the combined 7-GeV/c π^-p and π^+d data with $M(\pi^+\pi^-) > 1.4$ GeV/c^2 to eliminate the overlap with ρ and f production. This cut is seen to reduce α slightly while leaving the same general dependence on M^*.

To study further the low-mass M^* system we examine the nucleon-nucleon scattering angle, $\cos\theta_{NN}$, as defined in Fig. 26(a). We must demand $M(\pi^+\pi^-) > 1.4$ GeV/c^2 if we want to observe features of the angular distributions which may be characteristic of the π-nucleon rather than the π-π system. The $\cos\theta_{NN}$ distributions for $M(\pi^+\pi^-) > 1.4$

TABLE IX. $\sigma(\pi^+n \rightarrow N^*\pi^+)$ at 6.95 GeV/c.

Δ or N^* mass (GeV/c^2)	$\sigma(N^* \rightarrow p\pi^-)$ (μb)
1.26 ± 0.015	32 ± 15
1.37 ± 0.02	28 ± 18
1.50 ± 0.02	26 ± 16
1.65 ± 0.02	33 ± 15

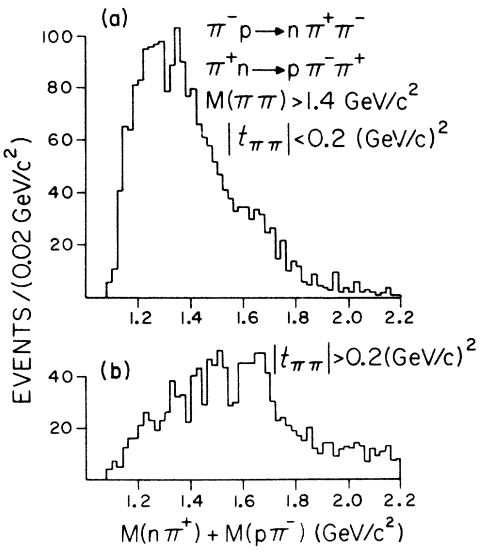

FIG. 24. $M(n\pi^+)$ and $M(p\pi^-)$ for combined $\pi^- p$ and $\pi^+ d$ data with $M(\pi^+\pi^-) > 1.4$ GeV/c^2. (a) $|t_{\pi\pi}| < 0.2$ (GeV/c)^2; (b) $|t_{\pi\pi}| > 0.2$ (GeV/c)^2.

GeV/c^2 are shown in Fig. 27. For $|t_{\pi\pi}| < 0.2$ (GeV/c)^2 the distributions are almost flat, especially in comparison with the large $|t_{\pi\pi}|$ data of Fig. 27(b). The small $t_{\pi\pi}$ data appear to be consistent with production via diffraction dissociation[55]; $\cos\theta_{NN}$ seems to be mostly S wave with the exception of $M^*(1.58-1.70)$. For $|t_{\pi\pi}| > 0.2$ (GeV/c)^2 $\cos\theta_{NN}$ is strongly peaked in the forward direction, and the data with $M^* < 1.4$ GeV/c^2 are suggestive of S-P wave interference. In the mass interval 1.4–1.46 GeV/c^2 the forward peak has become sharper indicating that D wave is becoming important. The distribution from 1.58–1.7 GeV/c^2 is most unusual, since in the backward direction it looks like a spin-flipped D wave and is fitted rather well by $\cos\theta\sin\theta \propto Y_2^1$. This situation is reminiscent of the A_2 which is also produced in a spin-flipped state.[17] Like the A_2 the structure from 1.58–1.7 GeV/c^2 also lies on the falling edge of a large diffractivelike background and is enhanced by discarding the small-momentum-transfer events.

VII. DEUTERON EFFECTS

Deuterium is often used in experiments as a means of obtaining a neutron target. Ordinarily one imagines that either the proton or the neutron is struck by the high-energy projectile and then escapes without further interaction. This picture of the interactions is probably moderately accurate. Looking at the momentum spectrum of the spectator protons, one can account for about 80–90% of the spectrum by means of the Hulthén wave function of the deuteron. Beyond a spectator momentum of ≈ 200 MeV/c other processes probably constitute a modest fraction of the nominally neutron events.

As an example of an effect that we have observed we show Figs. 28 and 29 in which the dipion mass spectrum from reaction (2) has been plotted for different cuts on the spectator momentum. For

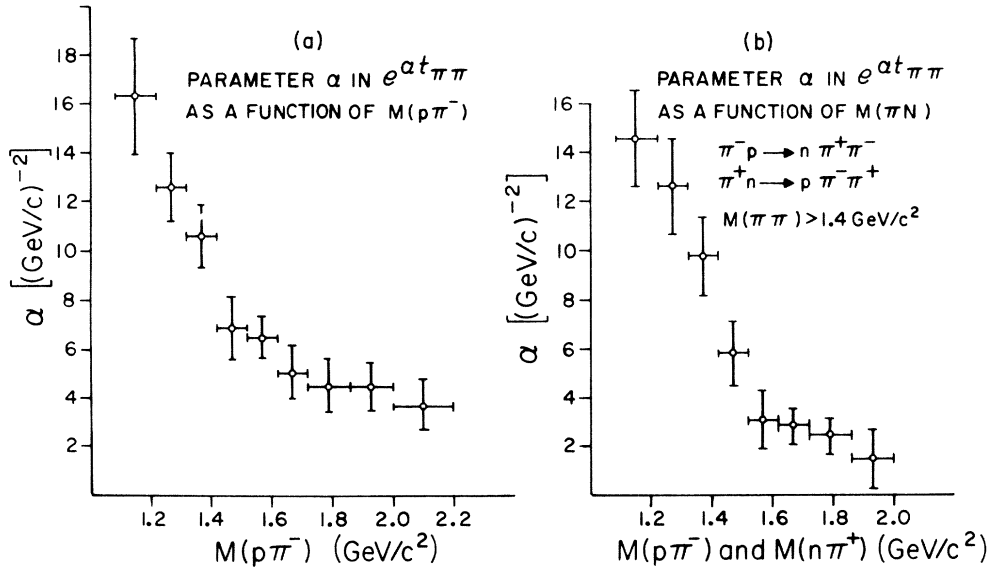

FIG. 25. Exponential slope parameter, α, from fits to the $t_{\pi\pi}$ distributions [fitting the data with $|t_{\pi\pi}| \lesssim 0.4$ (GeV/c)^2]. (a) Variation of α with $M(p\pi^-)$ for $\pi^+ d \to p_s p\pi^+\pi^-$; (b) variation of α for combined $\pi^- p$ and $\pi^+ d$ data with $M(\pi\pi) > 1.4$ GeV/c^2.

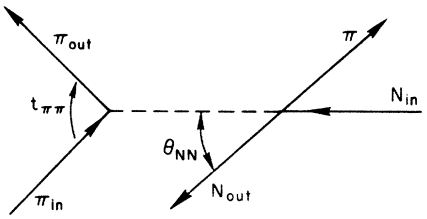

(a)

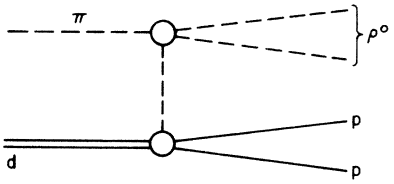

(b)

FIG. 26. (a) Diffractive scattering diagram showing the definition of $t_{\pi\pi}$ and the nucleon-nucleon scattering angle, θ_{NN}, defined in the center-of-mass frame of the π-nucleon system. (b) OPE diagram for $\pi d \to pp\pi\pi$.

the case of the invisible spectator the mass spectrum shows ρ^0, f^0, and g^0 peaks [Fig. 28(a)]. For visible spectator protons ($|\vec{p}_s| \gtrsim 80$ MeV/c) the g^0 has disappeared and the f^0 is slightly diminished as shown in Fig. 28(b). Figures 29(a) and 29(b) show $M(\pi^+\pi^-)$ and the ρ^0 decay angular distributions for events with $|\vec{p}_s| > 0.3$ GeV/c. In this case the f^0 is practically gone and only the ρ^0 is clearly visible. The angular distribution of the decay of the ρ^0 shows a dominance of the ρ_{00} moment of the distribution which is characteristic of the OPE process. The problem is then how to account for an OPE dominated process and a high-energy spectator.

A possible explanation of the effects observed can be given by considering the diagram shown in Fig. 26(b). In this case the virtual π^+ from the upper vertex is absorbed by the deuteron producing a diproton state. The cross section at the pion pole is given by the usual expression for the OPE process:

$$\frac{d^3\sigma}{dm^* dM^* dt} = \frac{1}{4\pi^3 P_0^2 E^2}(Km^{*2}\sigma_{\pi-\pi}) \times \frac{1}{(t-m_\pi^2)^2}(PM^{*2}\sigma_{\pi-d}),$$

where

P_0, E = center-of-mass momentum and energy,

$m^*, M^* = \pi$-π and p-p invariant mass,

K, P = virtual π momentum in $\pi^+\pi^-$ and πd center-of-mass systems,

and $\sigma_{\pi-\pi}, \sigma_{\pi-d}$ are the "on the mass shell" cross sections for π-π and $\pi d \to pp$ interactions. Figure 30 shows our observed diproton distribution. We show also the distribution expected on the basis of the Hulthén distribution and the distribution

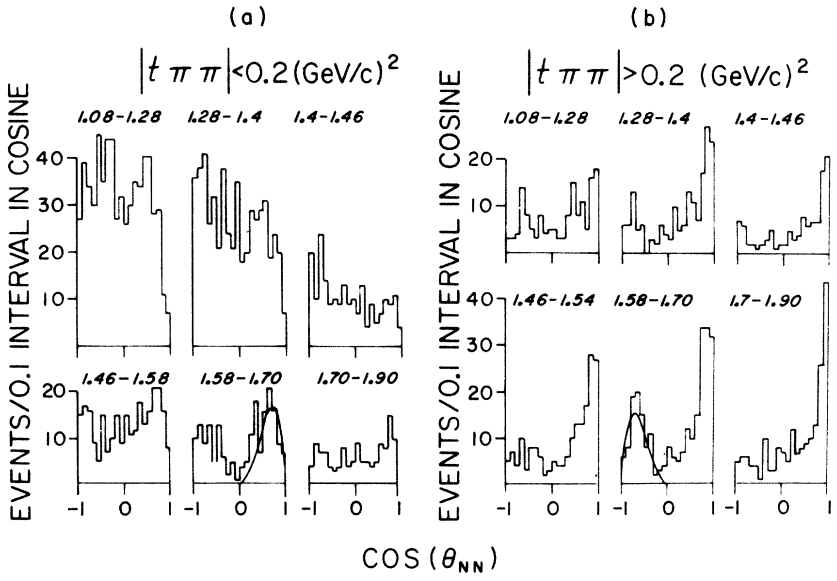

FIG. 27. cosθ_{NN} distributions for the $\pi^- p$ and $\pi^+ d$ data in intervals of $M(\pi$ nucleon) as shown. (a) Data with $|t_{\pi\pi}| < 0.2$ (GeV/c)^2; (b) data with $|t_{\pi\pi}| > 0.2$ (GeV/c)^2. θ_{NN} and $t_{\pi\pi}$ are defined in Fig. 26(a), and $M(\pi\pi) > 1.4$ GeV/c^2. The curves show cosθ sinθ distributions.

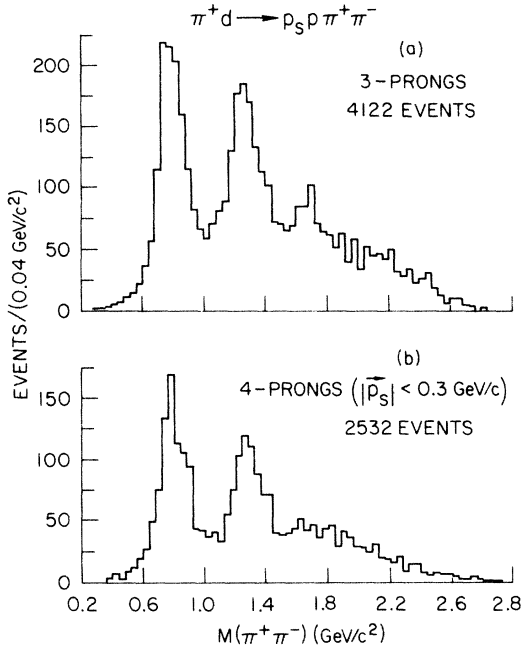

FIG. 28. $M(\pi^+\pi^-)$ from $\pi^+ d \rightarrow p_s p \pi^+ \pi^-$. (a) 3-prong events; (b) 4-prong events with $|\vec{p}_s| < 0.3$ (GeV/c).

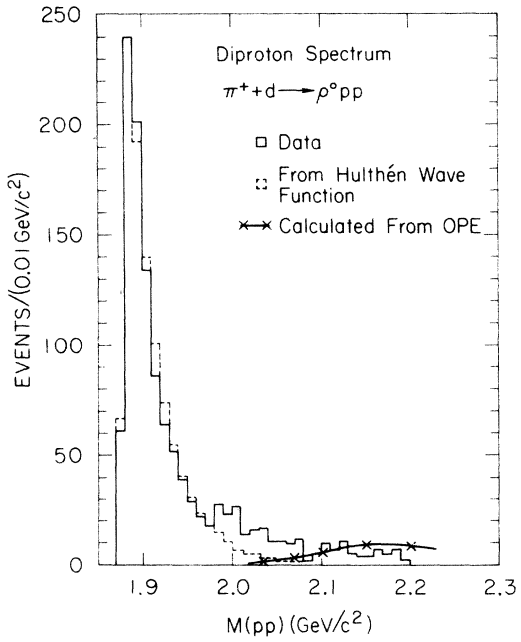

FIG. 30. The diproton mass spectrum, $M(pp)$, for the reaction $\pi^+ d \rightarrow pp p^0$. The curve is calculated using the OPE model.

calculated on the basis of the OPE cross section. The interesting feature of the process $\pi^+ d \rightarrow \rho^0 pp$ is that the reaction can go over a wide range of the diproton mass distribution with the virtual pion very close to the real pion, i.e., close to the pion pole. The curve shown on Fig. 30 is close to an absolute prediction. It was calculated using OPE and then normalized with respect to the observed process $\pi^+ p \rightarrow \rho^0 \Delta^{++}$. Beyond a diproton mass of 2.10 GeV/c^2 our experimental distribution is ≈30–40% low because of cuts made at the scanning level—correcting for this would tend to make the agreement better.

In Sec. V on ρ-ω interference we found a large difference in the mass spectrum depending on whether or not one observed a spectator. This effect is perhaps larger than can be accounted for by differences in resolution. It is possible that here we are also observing specifically dinucleon effects.

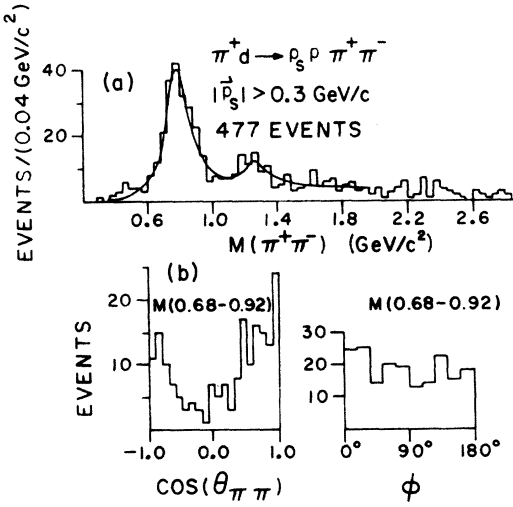

FIG. 29. The reaction $\pi^+ d \rightarrow p_s p \pi^+ \pi^-$ with $|\vec{p}_s| > 0.3$ GeV/c. (a) $M(\pi^+\pi^-)$; (b) $\cos\theta_{\pi\pi}$ and azimuthal angle distributions in the ρ^0 mass region.

VIII. CONCLUSIONS

From AOPE model fits to the $\pi^+\pi^-$ angular distributions we find strong evidence of resonant behavior in the $I=0$ S wave near the f^0 peak. There is a rapid change in η_S^0 for $1.0 < M(\pi\pi) < 1.2$ GeV/c^2, while near the f^0 peak $\eta_S^0 \simeq 1$ and $\delta_S^0 \simeq 270°$ implying a large imaginary S-wave amplitude. Our $2\pi^0$ data are consistent with this behavior. The $I=0$ D wave is significantly inelastic at the f^0 peak ($\eta_D^0 = 0.70$) and this observation is supported by estimates of non-2π f^0 decay modes. We find evidence for $\eta^0\eta^0$ and $\pi^+\pi^-\pi^0\pi^0$ decay modes of the f^0. The branching ratio for this 4π decay mode is not consistent with that one would predict from $f^0 \rightarrow \pi^+\pi^+\pi^-\pi^-$ assuming the decay proceeds through a $\rho\rho$ intermediate state.

We observe constructive ρ-ω interference in $\pi^+ n \rightarrow p\pi^+\pi^-$ in disagreement with most current theories. In the π-nucleon mass spectra there

are small signals from N^* production superimposed on an OPE background. Finally the events with $|\vec{p}_s| \gtrsim 0.3$ GeV/c show evidence of specifically deuteron effects in the OPE process.

ACKNOWLEDGMENTS

It is a pleasure to thank the operating staff of the ANL-MURA 30-in. bubble chamber under the direction of Dr. L. Voyvodic. We sincerely appreciate the fine work of the Toronto and Wisconsin scanning and measuring staffs. We are most grateful for the assistance of Dr. R. N. Diamond and Dr. J. T. Lynch on this experiment, and we thank Professor L. Durand, Professor A. R. Erwin, and Professor M. A. Thompson at the University of Wisconsin for helpful discussions. Finally, we thank W. M. Yeager at Duke University for his assistance with the data presented in this paper.

APPENDIX: $2\pi^0$ FITTING WITH γ's

In this appendix we discuss the procedure we used to fit the reaction $\pi^+ d \to p_s p \pi^0 \pi^0$ using the measured γ directions. Our method is basically the same as that used by Morse to study the reaction $\pi^- p \to p \pi^- \pi^0 \pi^0$ at 7 GeV/c.[56] We also discuss an analysis of this fitting procedure using Monte Carlo generated events.

As part of our normal scanning procedure all events were checked for associated γ's in the two tantalum (Ta) plates and in the deuterium. All 2-prong reaction (1) events were also checked a second time by γ editors, who were experienced scanners with special training concerning the use of the Ta plates to detect γ's. All γ's were classified as either "definite" or "questionable" depending on how well the γ pointed at the vertex of the event, whether or not the origin of the γ was ambiguous between two or more vertices, etc. Our procedure in fitting was never to discard definite γ's, e.g., a 3γ event with two definite γ's would be fitted to $\pi^0\pi^0$ using all 3 γ's and using only the two definite γ's. Approximately 54% of the γ's measured were definite.

Since we have only measured the γ directions as two point tracks we loose one constraint for each γ produced. Consequently unless we observe all 4 γ's from the decay of two π^0's we must make some approximations in order to fit the event. The approximations we make are based on well-known kinematic features of the decay $\pi^0 \to \gamma\gamma$. The opening angle θ from the decay of a π^0 of mass μ and momentum p_π satisfies the inequality

$$\tan\tfrac{1}{2}\theta \geq \mu/p_\pi .$$

From the opening-angle distribution,[57]

$$W(\theta) = \frac{1-v^2}{2v} \frac{\cos(\frac{1}{2}\theta)}{\sin^2(\frac{1}{2}\theta)} [v^2 - \cos^2(\tfrac{1}{2}\theta)]^{-1/2}$$

we compute the probability $P(\theta)$ that a π^0 of velocity v will decay into two γ's with an opening angle θ or larger,

$$P(\theta) = 1 - \frac{[v^2 - \cos^2(\frac{1}{2}\theta)]^{1/2}}{v \sin(\frac{1}{2}\theta)} .$$

As shown in Fig. 31(a), $P(\theta)$ is sharply peaked toward the minimum opening angle $\theta_{\min}$, and consequently if we know the π^0 momentum we can make a good estimate of the probable γ-γ opening angle. Conversely, if we have a measure of the opening angle for a particular $\pi^0 \to \gamma\gamma$ decay we can estimate the π^0 momentum. We define $P(p_\pi)$ to be the probability that the π^0 momentum will be p_π or larger for a given minimum momentum $p_{\min}$. In Fig. 31(b) we have plotted $P(p_\pi)$ as determined from Monte Carlo generated $2\pi^0$ events. The sharp peaking results partly from the kinematic restrictions of this experiment, i.e., as $p_{\min}$ increases the allowed values of p_π are restricted by the finite amount of missing momentum ($\approx$6.6 GeV/c). With this introduction we proceed to discuss the $2\pi^0$ fitting procedure for events with 1, 2, or 3 measured γ's; see Refs. 10, 48, and 56 for additional details.

1. 1γ events

For events with one measured γ we made a 0-constraint fit by pointing π_1^0 in the direction of the measured γ and allowing the fitting program to calculate the momentum of π_1^0 and the direction and momentum of π_2^0. A diagram of this situation is shown in Fig. 32(a). Since this is only a calculation there is little or no discrimination against events with more than two π^0's, however, the following factors speak in favor of this procedure. For events with MM $\lesssim 1.0$ GeV/c^2 the only appreciable $3\pi^0$ contribution comes from $\eta^0 \to 3\pi^0$. Second, if we see only 1γ from a $2\pi^0$ event it is likely to have come from the more energetic of the two π^0's. A 4 GeV/c π^0 has $\frac{1}{2}\theta_{\min} \simeq 1.93°$ and the probability is only 0.13 for $\theta > 2\theta_{\min}$ [see Fig. 31(a)], so pointing the π^0 in the γ direction will often be a good approximation. In analyzing these events we have demanded that the calculated momentum of π_1^0 be larger than the lower limit imposed by our estimate of the γ energy. Finally, the most convincing argument for using these 1γ events is that their fitted $M(\pi^0\pi^0)$ and angular distributions are similar to the 2γ-3γ-4γ events. The most obvious difference between the 1γ and the 2γ-3γ-4γ fits is that the former have slightly more events with

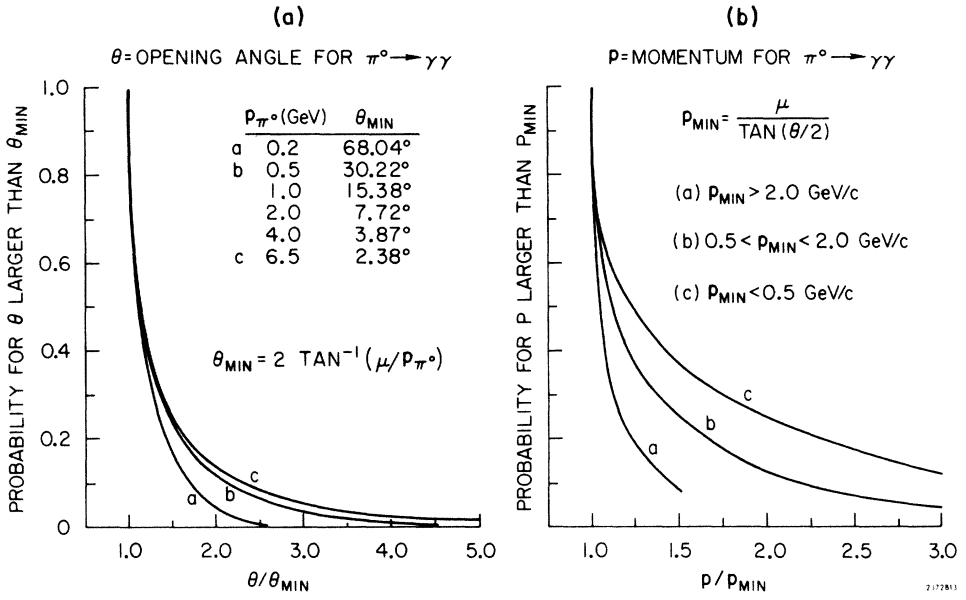

FIG. 31. (a) Probability that the $\gamma\gamma$ opening angle θ for $\pi^0 \rightarrow \gamma\gamma$ will be larger than the minimum opening angle θ_{min} for various π^0 momenta (μ = pion mass). (b) Probability that the π^0 momentum p for $\pi^0 \rightarrow \gamma\gamma$ will be larger than the minimum momentum p_{min} for a given $\gamma\gamma$ opening angle θ. The curves are Monte Carlo results for p_{min} in the indicated intervals.

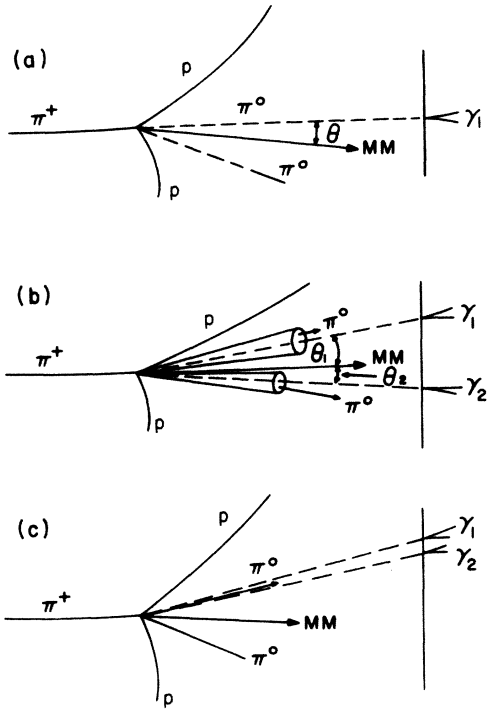

FIG. 32. π^0 direction assignments for kinematic fitting using measured γ directions. (a) One γ observed from π_1^0 and none from π_2^0; (b) one γ observed from each π^0; (c) two γ's observed from π_1^0 and none from π_2^0. MM denotes the missing momentum in $\pi^+ d \rightarrow pp$ + neutrals.

$M(\pi^0\pi^0) > 1.5$ GeV/c^2 and show a somewhat stronger D wave at the f^0 peak.

2. 2γ and 3γ events

For 2γ events there are two possibilities to consider: type 1—one γ from each π^0 is observed [see Fig. 32(b)]; type 2—two γ's from one π^0 and none from the other are detected [Fig. 32(c)].

For type 1 events we began by taking the π^0 directions to be the same as the γ directions and solve for the π^0 momenta using the angles θ_1 and θ_2 between the π^0 directions and the missing momentum ($= P_M$):

$$p_1 \cos\theta_1 + p_2 \cos\theta_2 = P_M,$$

$$p_1 \sin\theta_1 - p_2 \sin\theta_2 = 0.$$

Using these estimates of the π^0 momenta we determine the corresponding minimum opening angle θ_{min} for each π^0 and constrain the π^0 directions to lie within cones of half-angle $1.25\theta_{min}/2$. Actually it might be more correct to constrain the directions to lie within conical shells but the standard bubble-chamber kinematic fitting programs are not amenable to this type of a constraint. We also constrain the π^0 momentum to be $p_{int} \pm 0.2 p_{int}$ where p_{int} is the initial guess.

For type 2 events, two γ's from one π^0, we take the initial π_1^0 direction along the bisector of the two γ's and calculate the minimum π_1^0 momentum

from the γ-γ opening angle,

$$p_{\min} = \frac{\mu}{\tan\frac{1}{2}\theta}.$$

As shown in Fig. 31(b) the actual π^0 momentum is usually only slightly larger than the minimum, especially for fast π^0s. The π_1^0 momentum was constrained to be $\approx 1.1 p_{\min} \pm 0.2 p_{\min}$. The π_1^0 direction was constrained to lie in the plane of the two γ's and allowed to vary between the γ directions in this plane. As an aid in discriminating between 2γ events of type 1 and type 2, we defined the angles α and β as follows:

P_M = missing momentum,

$$\alpha = \cos^{-1}[(\hat{\gamma}_1 \times \hat{\gamma}_2) \cdot \hat{P}_M], \quad 0 \leq \alpha \leq 180^\circ$$

$$\beta = \cos^{-1}[(\hat{\gamma}_1 \times \hat{P}_M) \cdot (\hat{\gamma}_2 \times \hat{P}_M)], \quad 0 \leq \beta \leq 180^\circ.$$

If γ_1 and γ_2 are actually associated with the event in question then α should be close to 90°. Distributions of α for both fitted $2\pi^0$ and Monte Carlo generated events are sharply peaked at $\alpha = 90^\circ$. The 2γ events of type 1 are all within $\alpha = 90^\circ \pm 12^\circ$, and 94% of the type 2 events are within $\alpha = 90^\circ \pm 12^\circ$. The azimuthal angle β is very useful in deciding between 2γ fits of type 1 and 2. Type 1 events are peaked toward $\beta = 180^\circ$, while type 2 events peak near $\beta = 0^\circ$ with β usually less than 90°. Our Monte Carlo studies indicate that this angle alone is sufficient to distinguish between type 1 and 2 for 0.94 of the fake events. This agrees well with a ratio of 0.93 for real events. We found these angles to be just as useful as the χ^2 for selecting the correct fit.

For 3γ events there are three possible permutations of the γ's corresponding to which pair of γ's is assumed to come from π_1^0. Consider the case in which γ_1 and γ_2 come from π_1^0 and γ_3 from π_2^0. Initially we take π_1^0 along the bisector of γ_1 and γ_2 and point π_2^0 in the direction of γ_3. Now we can solve for the π^0 momenta and find errors for the direction and momentum of π_2^0 just as for type 1 of the 2γ events. In fitting this hypothesis we demand $M(\gamma_1\gamma_2) = \mu$ and use the artificially constructed track for π_2^0.

3. γ detection efficiency

We have checked our γ fitting procedure with Monte Carlo generated events. There are two points of interest: (1) What is our γ detection efficiency, and (2) what is the program efficiency for fitting the $2\pi^0$ events? We should also consider the effect of the non-$2\pi^0$ background in the missing-mass spectrum. We will assume that this background is predominantly $3\pi^0$ for MM $\gtrsim M_\omega$.

Initially we consider the problem of our γ detection efficiency. There are two efficiencies of interest, the "geometrical detection efficiency" (GDE), and the "actual detection efficiency" (ADE). The GDE is a measure of the effective solid angle subtended by the plates and depends simply on the fraction of γ's which hit the plates. The ADE is the probability for detecting n out of N produced γ's from a given reaction. In addition to geometry it depends on the γ-conversion probability (which is a function of the incident photon energy) and the "survival probability" (P_s) of the $e^\pm$ pairs. P_s is the probability that the $e^\pm$ will escape from the Ta plates with enough energy to be detected.

To determine these efficiencies we generated Monte Carlo events of the type $\pi^+ d \to p_s p + n\pi^0$ with $n = 2$ or 3. The events were generated with t distributions of the form $e^{\beta t}$ with $\beta = 4.0$ and 2.2 $(\text{GeV}/c)^{-2}$ for $2\pi^0$ and $3\pi^0$ events, respectively. In Figs. 33(a) and 33(c) we plot the GDE for $2\pi^0$ and $3\pi^0$ events. Since the multi π^0 system has a net momentum of 6–7 GeV/c our GDE is very good. Here we have neglected the strong D wave in the π-π system above 1.0 GeV/c^2.

For each γ which hits the plates we decide in a random fashion whether or not it converts and if it converts whether or not it produces a visible $e^\pm$ shower (see Appendix B of Ref. 56 for details). The ADE for $2\pi^0$ and $3\pi^0$ events is shown in Figs. 33(b) and 33(d). Obviously we cannot hope to study the $2\pi^0$ system using only 4γ events. The problem is a low γ conversion probability; the survival probability is of secondary importance since most of the γ's are fast and $P_s = 1$ for $E_{e^\pm} \gtrsim 0.3$ GeV. The two $\frac{1}{8}$-in. Ta plates provide 2×0.76 radiation lengths yielding a conversion probability of ≈ 0.69 for $E_\gamma \gtrsim 1.0$ GeV (0.03 of the measured γ's converted in the deuterium). The increase in conversion probability for photons not incident normal to the plates is somewhat compensated for by a decrease in the survival probability.

The encouraging feature of Fig. 33(b) is that most of the $2\pi^0$ events produce at least one observable γ. The fraction of events with 0 γ's is less than 0.1 out to $M(\pi\pi) = 1.7$ GeV/c^2. For comparison, 10% of the 2-prong missing-mass events had no measured γ's (see Sec. II). In Table X we list the fraction of reaction (1) events with 1, 2, 3, and 4 γ's for various $M(\pi^0\pi^0)$ intervals (these ratios have not been corrected for 0γ events). For comparison we list the corresponding ratios for the total sample as predicted from our Monte Carlo study. The agreement is good considering that we have neglected the fitting program efficiency and the $3\pi^0$ background. The largest discrepancy, which is for the 3γ events, will be seen to be related to the fitting program efficiency.

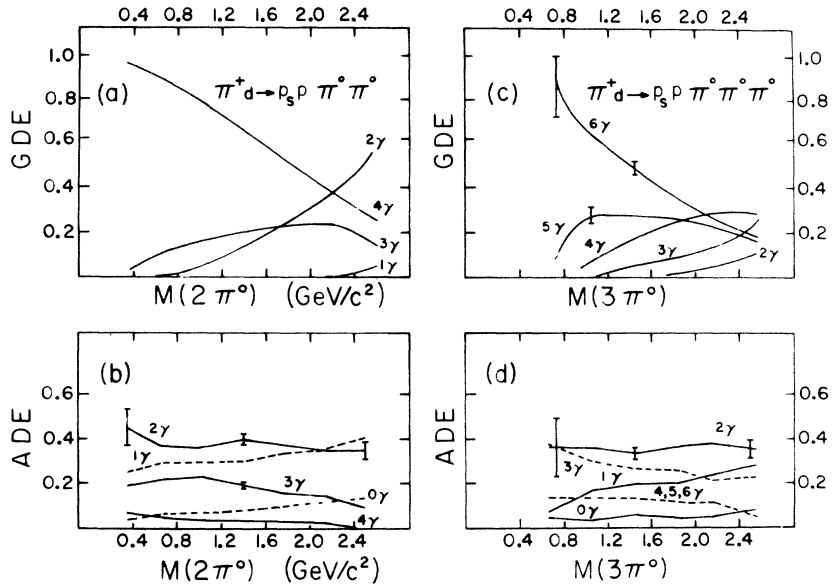

FIG. 33. Monte Carlo results for γ detection efficiencies. (a), (c) Geometrical detection efficiency (GDE) for $2\pi^0$ and $3\pi^0$ events; (b), (d) actual detection efficiency (ADE) for $2\pi^0$ and $3\pi^0$ events. Error bars are shown for a few of the data points.

4. Efficiency and resolution of $2\pi^0$ fitting

To check our procedure for reconstructing $2\pi^0$ events with less than four observed γ's we have used the Monte Carlo generated events as input to the reconstruction and kinematic fitting program. The events were processed through the $2\pi^0$ γ fitting programs using the same procedure as for real events. The program efficiency is defined to be the fraction of events which yield a good fit by the same criteria as used for real events. The efficiency for fake 2γ and 3γ events is given in Table XI. While the recovery rate for the $2\pi^0$ data is quite satisfactory, the discrimination against $3\pi^0$ events is low. The statistical uncertainty in the efficiency within the various mass intervals is typically ± 0.2. The reason for the rather low 3γ efficiency is not known. The χ^2 distributions for the fake $2\pi^0$ events are similar to those for real events whereas the $3\pi^0$ χ^2 distributions are rather flat. This would indicate a small $3\pi^0$ contamination in the real fitted events.

For 1γ events the program recovery rate is ≈ 1.0 for both $2\pi^0$ and $3\pi^0$ events, i.e., no discrimination against $3\pi^0$. The advantage of the fitting procedure for 1γ events is that we get some information on the π^0 directions. For $M(\pi\pi) \lesssim 1.4$ GeV/c^2 phase space alone yields some discrimination against $3\pi^0$. The fitting also gives little or no increase in mass resolution since the direction and momentum of the proton are usually much more tightly constrained than are the π^0's.

In Fig. 34 we compare the π^0 directions and momenta as reconstructed by the fitting program with the actual Monte Carlo generated π^0 directions (for $2\pi^0$ events). Figure 34(a) shows the angular resolution—the angle between the Monte Carlo generated and fitted π^0 direction for each event—for the various γ topologies. For the worst case of the 1γ events the resolution is $\approx 2^\circ$

TABLE X. Fraction of fitted and Monte Carlo $2\pi^0$ events in different γ topologies.

$M_{\pi\pi}$ (GeV/c^2)	1γ	2γ	2γ Type 1	2γ Type 2	3γ	4γ
min − 0.7	0.20	0.50	0.30	0.20	0.25	0.05
0.7 − 1.1	0.30	0.53	0.25	0.28	0.16	0.01
1.1 − 1.4	0.34	0.49	0.23	0.26	0.11	0.06
1.4 − 1.8	0.41	0.43	0.24	0.19	0.16	0.00
1.8 − max	0.62	0.37	0.14	0.23	0.01	0.00
Total	0.38	0.46	0.23	0.23	0.13	0.03
Monte Carlo	0.35	0.41	•••	•••	0.20	0.04

TABLE XI. Fraction of $2\pi^0$ and $3\pi^0$ Monte Carlo events with an acceptable $2\pi^0$ fit.

$M(^{2\pi^0}_{3\pi^0})$ (GeV/c^2)	$2\pi^0$ events 2γ	$2\pi^0$ events 3γ	$3\pi^0$ events 2γ	$3\pi^0$ events 3γ
min − 0.7	0.95	0.59	•••	•••
0.7 − 1.1	0.95	0.80	1.0	0.71
1.1 − 1.4	0.90	0.88	0.71	0.24
1.4 − 1.8	0.92	0.79	0.61	0.24
1.8 − max	0.83	0.81	0.39	0.06
Total	0.90 ± 0.1	0.79 ± 0.1	0.56 ± 0.1	0.30 ± 0.07

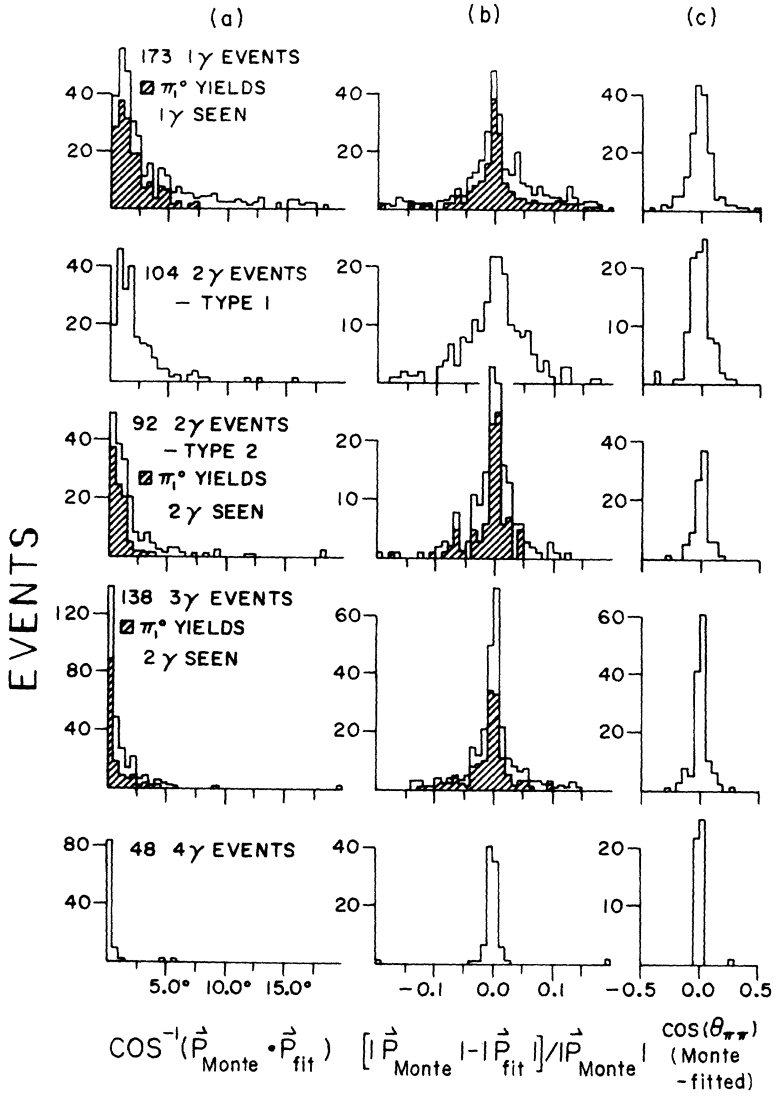

FIG. 34. Momentum and angular resolution for fitted $2\pi^0$ events with 1, 2, 3, and 4 γ's. $\vec{p}_{\text{Monte}}$ = Monte Carlo generated π^0 momentum, $\vec{p}_{\text{fit}}$ = momentum found by $2\pi^0$ fitting programs. (a) Laboratory angle between the Monte Carlo and fitted π^0 directions; (b) the fractional error in the magnitude of the fitted π^0 momentum; (c) difference in the π-π scattering angle, $\cos\theta_{\pi\pi}$ in the π-π center-of-mass frame, between the Monte Carlo and fitted $2\pi^0$ events.

in the laboratory frame of reference. For 3γ events the resolution is 1° or better. In Fig. 34(b) we plot the fractional difference between the Monte Carlo and fitted π^0 momentum. Again we see the progressive improvement as we go from one to four measured γ's. Two π^0 events of type 2 (2 γ's from 1 π^0) are seen to be more tightly constrained than type 1 events (1 γ from each π^0). Finally in Fig. 34(c) we plot the difference in $\cos\theta_{\pi\pi}$ as calculated for the Monte Carlo and fitted π^0 directions in the $\pi\pi$ center-of-mass system. For 1γ and 2γ–type 1 the resolution is ≈ 0.2 while for 2γ–type 2 and 3γ the resolution is at least 0.1. For 4γ events the resolution is smaller than the binning in the plot.

The above results indicate that our $2\pi^0$ fitting procedure allows us to recover useful information on the π^0 directions. While there is little if any improvement in mass resolution there is some discrimination against $3\pi^0$, especially for $M(3\pi) \gtrsim 1.2$ GeV/c^2. The fitting procedure does not produce any systematic shift of $M(\pi\pi)$ with respect to the missing mass. For $M(\pi\pi) > 1.0$ GeV/c^2 we find $M(\pi\pi)$ is always within 0.025 GeV/c^2 of the missing mass. The fitting procedure is rather insensitive to small changes in the error assignments for the π^0 directions and momenta.

*Work supported in part by the U. S. Atomic Energy Commission under Contracts No. AT(11-1)-881, No. AT(40-1)-3065, and by the National Research Council of Canada.

[1]R. J. Miller *et al.*, Phys. Rev. 178, 2061 (1969).
[2]L. W. Lovell, Ph.D. thesis, University of Michigan, 1968 (unpublished).
[3]A. Forino *et al.*, Phys. Lett. 19, 65 (1965).
[4]N. Armenise *et al.*, Nuovo Cimento 54, 999 (1968); Orsay-Bari-Bologna-Florence Collaboration, CERN Report No. 68-7, Vol. II (1968) (unpublished).
[5]F. Bruyant *et al.*, Phys. Lett. 10, 232 (1964); 12, 278 (1964).
[6]M. T. Fogli-Muciaccia and V. Picciarelli, Nuovo Cimento 8A, 670 (1972).
[7]J. R. Bensinger *et al.*, Phys. Lett. 36B, 134 (1971); K. J. Braun *et al.*, Phys. Rev. Lett. 21, 1275 (1968); K. J. Braun and D. B. Cline, Phys. Rev. D 8, 3794 (1974); G. A. Smith and R. V. Manning, Phys. Rev. 171, 1399 (1968).
[8]W. D. Apel *et al.*, Phys. Lett. 41B, 542 (1972); E. I. Shibata *et al.*, Phys. Rev. Lett. 25, 1227 (1970); A. Skuja *et al.*, *ibid.* 31, 653 (1973); M. Wahlig *et al.*, Phys. Rev. 147, 941 (1966).
[9]B. Y. Oh *et al.*, Phys. Rev. D 1, 2494 (1970). In Appendix B of this reference the factor of $(\alpha - \alpha')$ in Table II and Table III should be $(\alpha - \alpha')$, $\epsilon_1 = P/k_{\text{off}}$, and $\epsilon_0 = \gamma'\epsilon_1$.
[10]J. T. Carroll, Ph.D. thesis, University of Wisconsin, 1971 (unpublished).
[11]J. A. J. Matthews, Ph.D. thesis, University of Toronto, 1971 (unpublished).
[12]R. Hartung and D. Reeder, University of Wisconsin report, 1964 (unpublished).
[13]G. Giacomelli *et al.*, CERN Report No. CERN/HERA 69-1 (unpublished).
[14]M. A. Wahlig and I. Mannelli, Phys. Rev. 168, 1515 (1968).
[15]I. Butterworth *et al.*, Phys. Rev. Lett. 15, 734 (1965).
[16]J. D. Jackson, Nuovo Cimento 34, 1644 (1964).
[17]J. T. Carroll *et al.*, Phys. Rev. Lett. 25, 1393 (1970).
[18]J. T. Carroll *et al.*, Phys. Rev. Lett. 27, 1025 (1971); J. A. J. Matthews *et al.*, Nucl. Phys. B32, 366 (1971).
[19]We compare our results with the 5.1-GeV/c CERN data since, as of this writing, they have the best statistics of the published $\pi^+ d$ bubble-chamber experiments near our energy.
[20]Particle Data Group, Rev. Mod. Phys. 45, S1 (1973). See p. S74 for an extensive list of references on π-π scattering.
[21]For a complete review of π-π scattering see D. Morgan, notes of lectures given at the VII Finnish Summer School, Loma-Koli, 1972, Rutherford Laboratory report (unpublished); J. L. Petersen, Phys. Rep. 2C, 157 (1971); in π-π *Scattering—1973,* proceedings of the international conference on π-π scattering and associated topics, Tallahassee, 1973, edited by P. K. Williams and V. Hagopian (A.I.P., New York, 1973).
[22]J. P. Baton *et al.*, Phys. Rev. Lett. 33B, 528 (1970). See also J. P. Baton and G. Laurens, in *Proceedings of the Conference on $\pi\pi$ and $K\pi$ Interactions, Argonne National Laboratory, 1969,* edited by F. Loeffler and E. Malamud (ANL, Argonne, Ill., 1969).
[23]J. T. Carroll *et al.*, Phys. Rev. Lett. 28, 318 (1972).
[24]S. D. Protopopescu *et al.*, Phys. Rev. D 7, 1279 (1973).
[25]P. Estabrooks *et al.*, in π-π *Scattering—1973,* proceedings of the international conference on π-π scattering and associated topics, Tallahassee, 1973, edited by P. K. Williams and V. Hagopian (A.I.P., New York, 1973), p. 37.
[26]G. Grayer *et al.*, in *Experimental Meson Spectroscopy—1972,* proceedings of the third international conference on experimental meson spectroscopy, Philadelphia, 1972, edited by K-W. Lai and A. H. Rosenfeld (A.I.P., New York, 1972), p. 5.
[27]W. J. Robertson and W. D. Walker, Phys. Rev. D 7, 2554 (1973).
[28]C. Goebel, Phys. Rev. Lett. 1, 337 (1958).
[29]G. F. Chew and F. E. Low, Phys. Rev. 113, 1640 (1959).
[30]E. Ferrari and F. Selleri, Phys. Rev. Lett. 7, 387 (1961).
[31]H. P. Dürr and H. Pilkuhn, Nuovo Cimento 40, 899 (1965); J. Benecke and H. P. Dürr, *ibid.* 56, 269 (1968); G. Wolf, Phys. Rev. 182, 1538 (1969).
[32]K. Gottfried and J. D. Jackson, Nuovo Cimento 34, 735 (1964).
[33]L. Durand III and Y. T. Chiu, Phys. Rev. 139, B646 (1965).
[34]The AOPE model may overestimate the amount of absorption in the D wave. In order to obtain satisfactory fits for $\cos\theta \simeq \pm 1$ in the f^0 region we had to reduce the amount of $Y_2^1(\theta, \phi)$ in the expansions of the helicity amplitudes. We used values for the Y_2^1 terms 35% smaller than those predicted by the Durand-Chiu AOPE model. This correction lowered the fit χ^2 at the f^0 by $\approx 50\%$ while changing the fit results for the phase shifts by $\approx 10\%$.
[35]M. Baubiller *et al.*, contributed paper in *Proceedings of the XVI International Conference on High Energy Physics, Chicago-Batavia, Ill., 1972,* edited by J. D. Jackson and A. Roberts (NAL, Batavia, Ill., 1972); D. Cohen *et al.*, Phys. Rev. D 7, 661 (1973).
[36]V. Hagopian *et al.*, Phys. Rev. Lett. 14, 1077 (1965).
[37]E. Malamud and P. E. Schlein, Phys. Rev. Lett. 19, 1056 (1967); E. Malamud and P. E. Schlein, in *Proceedings of the Conference on $\pi\pi$ and $K\pi$ Interactions, Argonne National Laboratory, 1969,* edited by F. Loeffler and E. Malamud (ANL, Argonne, Ill., 1969).
[38]L. J. Gutay *et al.*, Phys. Rev. Lett. 18, 142 (1967).
[39]W. D. Walker *et al.*, Phys. Rev. Lett. 18, 630 (1967); W. D. Walker, Rev. Mod. Phys. 39, 695 (1967).
[40]J. A. J. Matthews *et al.*, Nucl. Phys. B33, 1 (1971); B. Hyams *et al.*, in π-π *Scattering—1973,* proceedings of the international conference on π-π scattering and associated topics, Tallahassee, 1973, edited by P. K. Williams and V. Hagopian (A.I.P., New York, 1973), p. 206.
[41]W. Beusch *et al.*, contributed paper in *High Energy Physics,* proceedings of the XV International Conference on High Energy Physics, 1970, edited by V. Shelest *et al.* (Naukova Dumka, Kiev, U.S.S.R., 1972).
[42]R. Diamond *et al.*, Phys. Rev. D 7, 1977 (1973). This paper includes $K\bar{K}$ data from this experiment. See also Y. Oren *et al.*, ANL report, 1972 (unpublished).
[43]J. V. Beaupré *et al.*, Nucl. Phys. B28, 77 (1971).
[44]J. C. Anderson *et al.*, Phys. Rev. Lett. 31, 562 (1973).
[45]At the f^0 peak $\eta = (1-R)/(1+R)$ where $R = \sigma_{\text{inelastic}}/\sigma_{\text{elastic}}$.
[46]M. Abramovich *et al.*, Nucl. Phys. B20, 209 (1970); W. W. M. Allison *et al.*, Phys. Rev. Lett. 24, 618 (1970); G. Goldhaber *et al.*, *ibid.* 23, 1351 (1969); S. Hagopian *et al.*, *ibid.* 25, 1050 (1970); B. N. Ratcliff

et al., Phys. Lett. 38B, 345 (1972).
[47]A. S. Goldhaber, G. C. Fox, and C. Quigg, Phys. Lett. 30B, 249 (1969). See also M. Gourdin *et al.*, *ibid.* 30B, 347 (1969); D. Horn, Phys. Rev. D 1, 1421 (1970).
[48]J. R. Bensinger, Ph.D. thesis, University of Wisconsin, 1970 (unpublished).
[49]D. S. Ayres *et al.*, in π-π *Scattering—1973*, proceedings of the international conference on π-π scattering and associated topics, Tallahassee, 1973, edited by P. K. Williams and V. Hagopian (A.I.P., New York, 1973), p. 284.
[50]J. A. J. Matthews *et al.*, Phys. Rev. Lett. 26, 400 (1971).
[51]C. Quigg, LBL Report No. LRL-UCID-3413, 1969 (unpublished).
[52]L. D. Roper, Phys. Rev. Lett. 12, 340 (1964); P. Bareyre *et al.*, Phys. Lett. 18, 342 (1965).
[53]W. D. Walker *et al.*, Phys. Rev. Lett. 20, 133 (1968).
[54]E. W. Anderson *et al.*, Phys. Rev. Lett. 25, 699 (1970).
[55]M. L. Good and W. D. Walker, Phys. Rev. 120, 1857 (1960); B. Y. Oh and W. D. Walker, Phys. Lett. 28B, 564 (1969).
[56]R. Morse, Ph.D. thesis, University of Wisconsin, 1969 (unpublished).
[57]G. Källén, *Elementary Particle Physics* (Addison-Wesley, Reading, Mass., 1964), p. 33.